

Confinement models for high strength short square and rectangular concrete-filled steel tubular columns

Farhad Aslani^{*1,2}, Brian Uy^{2,3a}, Ziwen Wang^{2b} and Vipul Patel^{4c}

¹ School of Civil, Environmental and Mining Engineering,
The University of Western Australia, Crawley, WA 6009, Australia

² Centre for Infrastructure Engineering and Safety,
The University of New South Wales, Sydney NSW 2052, Australia

³ School of Civil Engineering, The University of Sydney, Sydney, NSW 2006, Australia

⁴ School of Engineering and Mathematical Sciences, College of Science,
Health and Engineering, La Trobe University, Bendigo, VIC 3552, Australia

(Received July 07, 2016, Revised October 25, 2016, Accepted October 28, 2016)

Abstract. While extensive efforts have been made in the past to develop finite element models (FEMs) for concrete-filled steel tubular columns (CFSTCs), these models may not be suitable to be used in some cases, especially in view of the utilisation of high strength steel and high strength concrete. A method is presented herein to predict the complete stress-strain curve of concrete subjected to tri-axial compressive stresses caused by axial load coupled with lateral pressure due to the confinement action in square and rectangular CFSTCs with normal and high strength materials. To evaluate the lateral pressure exerted on the concrete in square and rectangular shaped columns, an accurately developed FEM which incorporates the effects of initial local imperfections and residual stresses using the commercial program ABAQUS is adopted. Subsequently, an extensive parametric study is conducted herein to propose an empirical equation for the maximum average lateral pressure, which depends on the material and geometric properties of the columns. The analysis parameters include the concrete compressive strength ($f'_c = 20 - 110 \text{ N/mm}^2$), steel yield strength ($f_y = 220 - 850 \text{ N/mm}^2$), width-to-thickness (B/t) ratios in the range of 15-52, as well as the length-to-width (L/B) ratios in the range of 2-4. The predictions of the behaviour, ultimate axial strengths, and failure modes are compared with the available experimental results to verify the accuracy of the models developed. Furthermore, a design model is proposed for short square and rectangular CFSTCs. Additionally, comparisons with the prediction of axial load capacity by using the proposed design model, Australian Standard and Eurocode 4 code provisions for box composite columns are carried out.

Keywords: composite columns; flexural stiffness; reliability analysis

1. Introduction

Concrete-filled steel tubular columns (CFSTCs) have seen increased usage in modern construction practices throughout the world. This growth in use is largely due to the structural and

*Corresponding author, Senior Lecturer, Ph.D., E-mail: farhad.aslani@uwa.edu.au

^a Professor, Ph.D., E-mail: b.uy@unsw.edu.au

^b Master Student

^c Lecturer, E-mail: v.patel@latrobe.edu.au

economical benefits offered by concrete-filled steel tubes over hollow sections, as well as their aesthetic appeal when compared with I-sections. From a structural perspective, hollow sections exhibit high torsional and compressive resistance about both principal axes when compared with open steel sections. Moreover, the exposed surface area of a closed section is almost two-thirds that of a similar sized open section, thus requiring reduced painting and fireproofing costs (Packer and Henderson 2003). Composite columns comprise a combination of concrete and steel and utilise the most favourable properties of the constituent materials. Use of composite columns can result in significant savings in column size, which eventually can lead to substantial economic savings. This reduction in column size is particularly beneficial where floor space is at a premium, such as in car parks and multi-storey office buildings (Lam and Gardner 2008). The performance of CFSTCs can be further improved if high-strength materials are used. High-strength steel and concrete are considered to be effective alternatives to normal-strength steel and concrete for multi-storey and high-rise construction (Aslani *et al.* 2015a, b).

It is well known that CFSTCs with circular, square and rectangular steel cross-sections have been frequently used in numerous engineering structures owing to their excellent structural behaviour. In the past, many studies on these types of columns have been conducted. Some new types of CFSTCs have been considered in recent years (Aslani *et al.* 2016). Han *et al.* (2005) evaluated the compressive behaviour of inclined, tapered, and straight-tapered short CFSTCs. Yang *et al.* (2008) investigated the behaviour of elliptical short CFSTCs. Chen and Shen (2010) studied the behaviour of L-shaped CFSTCs under axial loading. Yang *et al.* (2010) reported experimental research of T-shaped CFSTCs under axial loading. Ren *et al.* (2014) studied the behaviour of axially loaded short CFSTCs with triangular, fan-shaped, D-shaped, quadri-circular, and semi-circular cross-sections. Hence, the performance of CFSTCs is affected by the sectional shape, width-to-thickness ratio, concrete compressive strength, and steel yield strength. Experimental studies can be conducted for examining the effects of many parameters on the behaviour of CFSTCs. However, experimental studies are costly and time consuming. Numerical studies can be effectively employed for conducting extensive parametric studies. These numerical studies with proper calibration depend on the accurate concrete confinement model for predicting reliable results. Significant experimental and numerical studies have been carried out to predict the behaviour of CFSTCs. For numerical studies, finite element models (FEMs) are often used for simulating the behaviour of CFSTCs. Material constitutive models used in the FEM analysis of CFSTCs can have a major influence on the precision of the predicted behaviour. Concrete confinement models of square and rectangular CFSTCs have been proposed by many researchers. However, discrepancies in the existing confining pressure models have been found. Therefore, the aim of this paper is to develop a generic concrete confinement model for the accurate characterisation of the behaviour of normal and high strength short square and rectangular short CFSTCs under axial compression.

Susantha *et al.* (2001) proposed an analytical approach based on existing experimental results and attempted to determine a complete uniaxial stress–strain law for confined concrete in CFSTCs. Three types of cross-sectional shapes such as circular, box and octagonal were considered. Their analytical approach was in predicting a complete uniaxial stress–strain law for normal strength confined concrete in CFSTCs. Hence, this paper extends Susantha *et al.*'s (2001) analytical approach to a generic concrete constitutive model for high strength short square and rectangular short CFSTCs under axial loading. Furthermore, a simplified confinement pressure versus width-to-thickness ratio model, appropriate confined concrete constitutive models, and an accurate FEM which incorporates the effects of initial local imperfections and residual stresses has been

developed. The predictions of the behaviour, ultimate strengths, and failure modes are compared with the available experimental results to verify the accuracy of the models developed. Moreover, a design model incorporating the proposed concrete confining pressure formula is proposed for predicting the ultimate axial strength of short square and rectangular short CFSTCs. The ultimate axial strengths for CFSTCs obtained from design codes, Australian Standard 5100.6 (2004), Eurocode 4 (2004) and the proposed design model, are compared with experimental results.

2. Previous research

Previously available research is classified under the following three sub-sections: (a) Normal-strength steel tube columns filled with high-strength concrete (NSS-TC-HSC); (b) High-strength steel tube columns filled with normal-strength concrete (HSS-TC-NSC); and (c) High-strength steel tube columns filled with high-strength concrete (HSS-TC-HSC).

2.1 NSS-TC-HSC

There are numerous experimental studies on high-strength CFSTCs, such as those carried out by Rangan and Joyce (1992), Kilpatrick and Rangan (1999a, b), and Johansson and Gylltoft (2001). Melcher and Karmazinova (2004) presented the test results of CFSTCs with high-strength concrete class between C55/67 and C80/95. Sakino *et al.* (2004) studied twenty HSC specimens with concrete strength between 77 and 91 N/mm² to study the behaviour of centrally loaded short CFSTCs. Han *et al.* (2005) tested fifty circular and square hollow structural steel stub columns infilled with self-compacting concrete of cube strengths between 50 and 90 N/mm².

For combined concentrically and eccentrically loaded behaviour, Liu (2004, 2005, 2006) performed a series of tests on HSC-filled rectangular steel tubular columns subjected to concentric and eccentric loading. The cylinder strengths of the HSC ranged between 60 and 90 N/mm². Yu *et al.* (2008) carried out a study on twenty-eight thin-walled hollow square and circular steel tubes infilled with self-consolidating concrete with cube strength of 122 N/mm². Portolés *et al.* (2011) determined that it was apparent that the use of HSC in slender concrete-filled tubular columns does not offer the same improvement as that of NSC in composite members where the stiffness does not increase proportionally to the increasing of compressive strength. In addition, Hernández-Figueirido *et al.* (2012) described thirty-six experimental tests conducted on rectangular CFSTCs filled with concrete up to 90 N/mm² and subjected to axial compression and different eccentricities at both ends. The tests showed that the use of high-strength concrete is more useful for the cases of non-constant bending moment since second order effects are reduced. However, when the aim is to obtain ductile behaviour, the use of NSC is considered more suitable.

2.2 HSS-TC-NSC

Uy (1999, 2001a) presented the results of steel and composite sections fabricated using high-strength structural steel of nominal yield stress 690 N/mm² and NSC of 20 N/mm². These cross-sections were conducted as short columns and were subjected to concentric axial compression. Uy (2001b) conducted an extensive experimental programme on short concrete-filled steel box columns, which incorporated high-strength structural steel of Grade 690 N/mm². The experiments were then used to calibrate a refined cross-sectional analysis method, which considered both the

non-linear material properties of the steel and concrete coupled with the measured residual stress distributions in the steel. Uy *et al.* (2002) conducted further research on high-strength steel box columns filled with concrete. This study consisted of three short columns and three slender columns to consider both the strength and stability aspects of steel-concrete composite high-strength composite columns.

Sakino *et al.* (2004) studied sixteen specimens with steel yield strengths between 507 and 853 N/mm² to investigate the behaviour of centrally loaded short CFSTCs, and proposed formulae to estimate the ultimate axial compressive capacities of CFSTCs. Mursi and Uy (2004, 2006a, b) carried out further experimental work on high-strength steel slender columns loaded uni-axially and bia-axially and assessed the applicability of existing codes of practice to deal with high-strength steel and NSC. Their findings established that existing codes of practice were quite conservative in dealing with these structural forms for biaxial loading in particular. Aslani *et al.* (2015a) presented the results of sixteen hollow and composite columns loaded in uniform concentric axial compression fabricated using high-strength structural steel of mean yield stress 701 N/mm² and concrete of 21–55 N/mm². In this study the confinement of the concrete is determined by summing the recorded transverse forces on the plate elements. Also, simplified confining pressure and maximum compressive strength of confined concrete models are proposed that can predict the confining pressure for the high strength CFSTCs.

2.3 HSS-TC-HSC

Fujimoto *et al.* (1995) reported an extensive set of tests on short square CFSTCs subjected to combined compression and bending. A total of twenty two specimens with steel yield stresses of 260 to 835 N/mm² and concrete cylinder strengths varying from 25 to 80 N/mm² were tested. Test results showed that the strength of the CFST beam-columns was considerably affected by the B/t ratio and the axial load level. In addition, the specimens containing high-strength steel exhibited lower ductility than those fabricated from normal-strength steel.

Liu *et al.* (2003) studied twenty-two short rectangular CFSTCs ($f_y = 550$ N/mm², and $f_c = 70 - 82$ N/mm²) subjected to concentric loading, it is distinguished that the strength of specimens reduced with the increase of cross-sectional aspect ratios. Sakino *et al.* (2004) studied fifteen specimens with concrete strength between 77 and 91 N/mm² and steel yield strength between 507 and 853 N/mm² to investigate the behaviour of centrally loaded short CFSTCs. Liu (2004, 2005, 2006) performed a series of tests on high-strength CFSTCs with concrete cylinder strength between 60 and 90 N/mm² and with steel yield strength between 495 and 550 N/mm².

Recently, Uy *et al.* (2013) presented an experimental investigation on CFSTCs with nominal yield strength of the steel sections of the columns as 690 N/mm², and the unconfined compressive strength of the inner concrete section of the CFSTCs with a range from 80 to 100 N/mm². Forty short specimens, with a length to width ratio of 3.5 and a width to thickness ratio of 15 to 40 were subjected to monotonic loading to investigate the ultimate strength, the local buckling effects and the confinement effects of the high-strength CFSTCs.

3. Experimental database

As outlined in Section 2, the experimental results are placed into three categories as follows: (a) NSS-TC-HSC; (b) HSS-TC-NSC; and (c) HSS-TC-HSC. Furthermore, this database is subdivided

into columns of “square, S” and “rectangular, R”. The information required and reported for each CFSTC test is: the width (B) of square and rectangular cross-sections, the thickness of the steel tube (t), length of the column (L), yield strength of the steel tube (f_y), and compressive strength of the concrete (f_c). In this paper high-strength steel is considered for steel tubes with $f_y \geq 450$ N/mm² and high strength concrete with $f_c \geq 60$ N/mm². Also, in order to better reflect the deviations of code predictions from the experimental results, the -10% and +10% error bounds are provided in the figures presented in the following sub-sections.

Furthermore, because the method to assess the compressive strength of concrete varied, the f_c values were corrected. In this study, compressive strength of concrete cylinder specimens with 150×300 mm dimension were considered as the default and the other types of specimens are converted by using conversion factors proposed by Yi *et al.* (2006). The concrete strength conversion factors are between cylinder specimens with 100×200 mm and 150×300 mm dimensions, cube specimens with 100 mm and 150 mm dimensions, and prism specimens with 150×150×300 mm dimension. Yi *et al.* (2006) and Aslani (2013) proposed conversion factors for high- and normal-strength concrete as shown in Table 1. The range of collected CFSTCs test properties is provided in Table 2.

Table 1 Compressive concrete strength conversion factors

For high strength concrete	$f_{cy(150 \times 300)}$	$f_{cu(100)}$	$f_{cu(150)}$	$f_{cpr(150)}$
$f_{cy(100 \times 200)}$	1.04	0.96	1.02	1.11
$f_{cy(150 \times 300)}$	1.00	0.92	0.98	0.94
For normal strength concrete	$f_{cy(150 \times 300)}$	$f_{cu(100)}$	$f_{cu(150)}$	$f_{cpr(150)}$
$f_{cy(100 \times 200)}$	1.03	0.85	0.91	1.07
$f_{cy(150 \times 300)}$	1.00	0.82	0.88	1.05

Table 2 Experimental results database properties

Properties range	Square column type		
	NSS-TC-HSC	HSS-TC-NSC	HSS-TC-HSC
B (mm)	60-211	110-240	60-211
B/t	20-39	20-40	20-40
L (mm)	180-633	300-720	180-700
f_c (N/mm ²)	61-106	20-55	60-98
f_y (N/mm ²)	262-347	495-835	404-835
No. of tests	22	37	29
Properties range	Rectangular column type		
	NSS-TC-HSC	HSS-TC-NSC	HSS-TC-HSC
B (mm)	100-220	90-230	80-200
B/t	17-41	19-48	19-50
L (mm)	300-348	450-690	300-600
f_c (N/mm ²)	66-106	30-55	60-89
f_y (N/mm ²)	300-380	495-730	486-550
No. of tests	30	9	31

4. Finite element analysis

The FEM program ABAQUS (2013) was used in this study to develop an accurate FEM for predicting the behaviour of short square and rectangular CFSTCs under axial loading. For the purposes of accurate FEM analysis, element type, element mesh, boundary condition, steel tube–concrete interface, material properties for steel tube and confined concrete, initial imperfections and residual stresses must all be considered. Typical cross-sections of square and rectangular CFSTCs are depicted in Fig. 1.

4.1 Element type, element mesh and boundary condition

The steel tube is characterised by four-node thick reduced integration shell elements with six degrees of freedom at each node (S4R). In the meantime, the concrete core of the CFSTCs was modelled using eight-node reduced integration brick elements with three translational degrees of freedom at each node (C3D8R) (Aslani *et al.* 2015a), as shown in Fig. 1.

The mesh size of the FEM was an important issue in tracing the softening behaviour of CFSTCs. Therefore, a study was carried out to establish mesh convergence to provide a rational mesh size which provided consistent results with the least computational time. Based on the mesh convergence study, the smallest and largest element sizes were chosen as $B/23$ and $B/13$, respectively, with B representing the width of the steel sections (Aslani *et al.* 2015a, 2017).

Fixed boundary conditions were applied to tie the end section surface to the reference point located at the centre of the end section (Aslani *et al.* 2015a). The end sections are planar during the analysis with these boundary conditions and consequently it was not essential to take into account the end plates or stiffeners in the model. The clamped condition (i.e., fixing all degrees of freedom except for the displacement at the loaded end) was used in this study. Symmetric boundary conditions were also applied to the surfaces at the symmetric planes of the column.

4.2 Influence of initial imperfections and residual stresses

As initial imperfections are considered in the present model, an eigenvalue buckling analysis was first undertaken to provide the lowest buckling mode to be used as the shape of the initial imperfection in following the load-deflection nonlinear analysis as shown in Fig. 2. The ultimate axial strength and post-buckling behaviour of CFSTCs was then achieved from the nonlinear load-deflection analysis. The magnitude of the initial imperfection was introduced by means of an induced displacement at the mid-height of the plate, which varies from $0.0005B$ to $0.005B$. The magnitude of the initial imperfection was taken as $0.001B$ (Aslani *et al.* 2015a, Chen *et al.* 2012).

An accurate and reliable treatment of residual stresses is vital for both numerical simulations and design theories especially for high-strength steel CFSTCs. The distribution of residual stress of the steel box columns contains a combination of internal residual compressive and tensile stresses which balance each other out axially as there is no axial restraint. The magnitude of the residual compressive stress in this study was assumed to be approximately 10% of the yield stress (Aslani *et al.* 2015), as shown in Fig. 1.

4.3 Steel tube-concrete interface

The steel tube and concrete interface is simulated by using surface-to-surface contact. The outer surface of the concrete infill and the inner surface of the steel tube are used as a contact surface

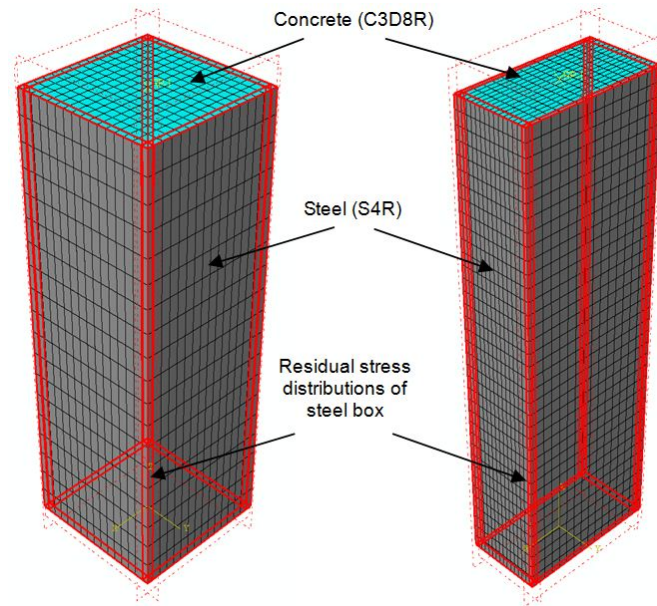


Fig. 1 Full FEM model of square and rectangular CFSTCsd

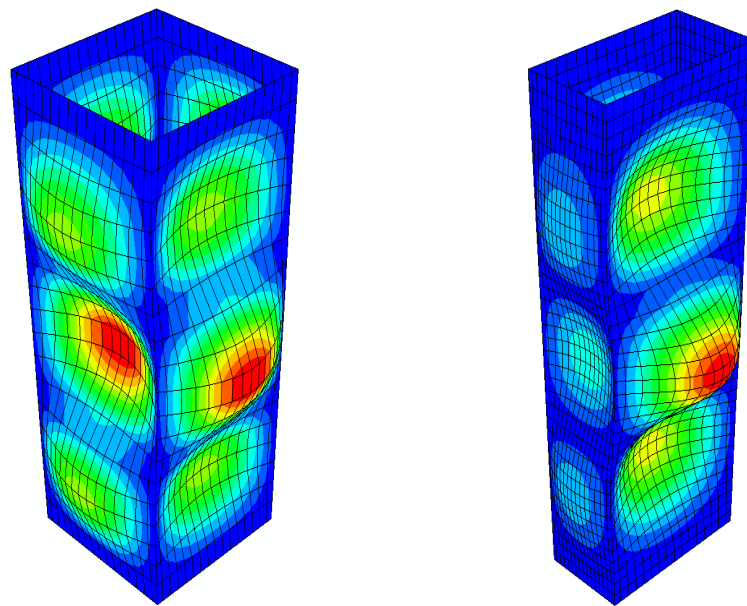


Fig. 2 Typical first buckling mode shape

pair. “Hard contact” in the normal direction can be specified for the interface, which permits the separation of the interface in tension and no penetration of that in compression. The tangential behaviour between the steel tube and concrete is simulated by the Coulomb friction model with a friction coefficient taken as 0.6 (Aslani *et al.* 2015a, 2017).

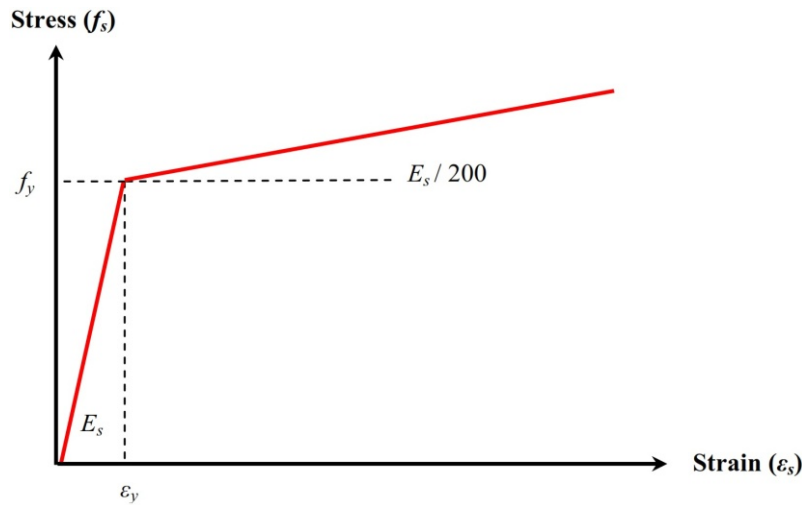


Fig. 3 Stress–strain curve for steel tubes

4.4 Material properties for the steel tube and confined concrete

4.4.1 Structural steel

Steel material properties specified in ABAQUS included the modulus of elasticity of the steel (E_s) taken as $200,000 \text{ N/mm}^2$ if E_s was not provided in the study and Poisson's ratio (ν_s) taken as 0.3. In this FEM the steel is assumed to behave as an elastic–plastic material with strain hardening in compression. For the elastic–plastic model as shown in Fig. 3 with linear strain hardening, the strain hardening modulus was taken as $E_s/200$ (Guo *et al.* 2007).

4.4.2 Confined concrete

The steel tube provides confinement to the concrete infill in CFSTCs under axial compression which increases the strength and ductility of the concrete infill. The confinement effect depends on the width-to-thickness ratio of the steel tube and material properties. By using the FEM analysis, strength improving at the state of tri-axial loading can be achieved by the definition of the yielding surface, and the description of the plastic behaviour coming from the equivalent stress–strain relationships of the concrete infill (Aslani *et al.* 2015a). The damage plasticity model defined in ABAQUS is used in the analysis. Since CFSTCs are under monotonic axial compression, damage variables were not defined. Therefore, concrete non-linearity was modelled as plasticity only.

Concrete material parameters required to be defined included modulus of elasticity (E_c), Poisson's ratio (ν_c), flow potential eccentricity (e), viscosity parameter, dilation angle (ψ), shape factor for yield surface (K_c), the ratio of initial equi-biaxial compressive yield stress to initial uniaxial compressive yield stress (f_{b0}/f_c), and equivalent stress–strain relationship for compression and tension sides, respectively.

The modulus of elasticity of the concrete was calculated as $E_c = 3320\sqrt{f'_c} + 6900$ which was suggested by ACI 318 (2010), where f'_c is in N/mm^2 and Poisson's ratio of $\nu_c = 0.20$ is adopted. Default values of 0.1 and 0 were used for the flow potential eccentricity and viscosity parameter, respectively. These two parameters have no significant influence on the prediction accuracy.

The ψ , K_c , f_{b0}/f_c can be determined as follows (Aslani *et al.* 2015a, 2017)

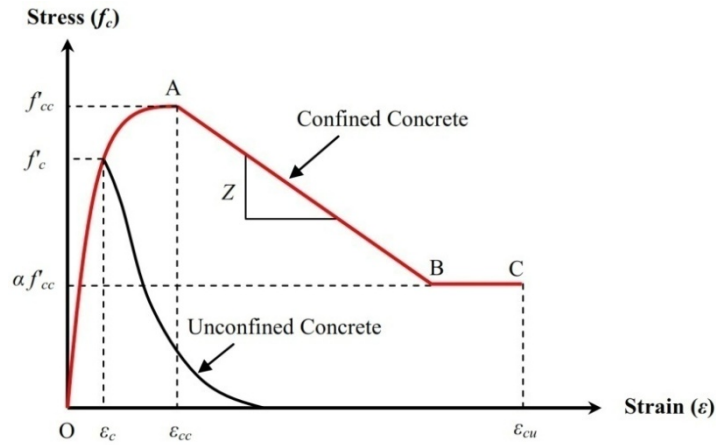


Fig. 4 Full FEM model of square and rectangular CFSTCs

$$\psi = 40^\circ \tag{1}$$

$$\frac{f_{b0}}{f'_c} = 1.5(f')^{-0.075} \tag{2}$$

$$K_c = \frac{5.5}{5 + 2(f'_c)^{0.075}} \tag{3}$$

Susantha *et al.*'s (2001) compressive equivalent stress-strain curve illustrated in Fig. 4 was used to simulate the material behaviour of confined concrete in CFSTCs. The non-linear ascending part of the curve OA ($0 < \varepsilon \leq \varepsilon_{cc}$) was modelled by equations recommended by Susantha *et al.* (2001), as Eqs. (4) to (10).

$$f_c = f'_{cc} \left[\frac{x r}{r - 1 + x^r} \right] \tag{4}$$

$$x = \frac{\varepsilon}{\varepsilon_{cc}} \tag{5}$$

$$r = \frac{E_c}{\left(E_c - \frac{f'_{cc}}{\varepsilon_{cc}} \right)} \tag{6}$$

$$\varepsilon_{cc} = \varepsilon_c \left[1 + 5 \left(\frac{f'_{cc}}{f'_c} - 1 \right) \right] \tag{7}$$

$$f'_{cc} = f'_c + m f_{rp} \tag{8}$$

$$f_{rp} = -6.5 R \frac{(f'_c)^{1.46}}{f_y} + 0.12 (f'_c)^{1.03} \quad (9)$$

$$R = \frac{B}{t} \sqrt{\frac{12(1-\nu_s^2)}{4\pi^2}} \sqrt{\frac{f_y}{E_s}} \quad (10)$$

Here, it should be pointed out that a constant reduction factor of 0.85 was adopted for the unconfined concrete strength when calculating the confined concrete compressive strength f'_{cc} . Hereafter, instead of f'_c , $0.85f'_c$ will be used for calculating f'_{cc} in Eq. (8).

The post-peak behaviour of the stress-strain curve AB ($\varepsilon_{cc} < \varepsilon \leq \varepsilon_{cu}$) was described to be linear for box section with a gradient of Z in Susantha *et al.* (2001), as Eqs. (11) to (13).

$$f_c = f'_{cc} - Z (\varepsilon - \varepsilon_{cc}) \quad (11)$$

$$Z = \begin{cases} 0 & R \frac{f'_c}{f_y} \leq 0.0039 \\ 23400 R \frac{f'_c}{f_y} - 91.26 & R \frac{f'_c}{f_y} > 0.0039 \end{cases} \quad (12)$$

$$\varepsilon_{cu} = \begin{cases} 0.04 & R \frac{f'_c}{f_y} \leq 0.042 \\ 14.50 \left[R \frac{f'_c}{f_y} \right]^2 - 2.4R \frac{f'_c}{f_y} + 0.116 & 0.042 < R \frac{f'_c}{f_y} \leq 0.073 \\ 0.018 & R \frac{f'_c}{f_y} \geq 0.073 \end{cases} \quad (13)$$

The upper limit of ε_{cu} should be satisfied by the following limitation (Susantha *et al.* 2001)

$$\varepsilon_{cu} \leq \varepsilon_{cc} + \frac{f'_{cc}}{Z} \quad (14)$$

The residual strength beyond ε_{cu} (i.e., part BC) is taken as a constant value which is proportional to the confined concrete strength as suggested by Susantha *et al.* (2001)

$$f_c = \alpha f'_{cc} \quad (15)$$

$$\alpha = 1 - \frac{Z (\varepsilon_{cu} - \varepsilon_{cc})}{f'_{cc}} \quad (16)$$

where f_c is the longitudinal compressive stress of the concrete in N/mm^2 , f'_{cc} is the compressive strength of the confined concrete in N/mm^2 , f'_c is the compressive strength of the unconfined concrete in N/mm^2 , f_{rp} is the maximum radial pressure on concrete in N/mm^2 , f_y is the yield strength of the steel in N/mm^2 , ε is the longitudinal compressive strain of the concrete, ε_{cc} is the strain at f'_{cc} , ε_c is the strain at f'_c , r is the material parameter that depends on the shape of the stress–strain curve, E_c is the Young's modulus of concrete in kN/mm^2 , E_s is the Young's modulus of steel in kN/mm^2 , B/t is the width-to-thickness ratio, and m is an empirical coefficient and assumed to be 4.0.

The tensile behaviour is assumed to be linear until the tensile strength is reached, which is taken as $f_{ct} = 0.56\sqrt{f'_c}$ suggested by ACI 318 (2010). Beyond this tensile stress, the tensile response is represented by means of a fracture energy approach defined by FIP (2010) and Bažant and Becq-Giraudon (2002) as follows

$$G_f = (0.0469d_{\max}^2 - 0.5d_{\max} + 26) \left(\frac{f'_c}{10} \right)^{0.7} \text{ N/m} \quad (17)$$

where f'_c is in N/mm^2 and d_{\max} is the maximum coarse aggregate size (in mm). If d_{\max} was not reported in a reference, it was taken to be 20 mm.

The FEM results suggest that the current used Susantha *et al.* (2001) model tends to overestimate the ultimate axial strength of the CFSTCs and it is not suitable for high strength CFSTCs. In this study an extensive parametric analysis has been carried out based on the approach of Aslani *et al.* (2015a) which proposes a simple empirical equation for calculating the confined concrete compressive strength. The main aim of the parametric analysis is to consider the various experimental parameters (i.e., unconfined concrete compressive strength, yield strength of the steel, and width-to-thickness ratio) on the confined concrete compressive strength and developing the rational and simple relationships that are in good correlation with test results.

Following the carrying out of the parametric analysis results, part OA of the stress–strain curve and confined concrete compressive strength were modified as outlined in the following, Eqs. (18) to (26)

$$f_c = f'_{cc} \left[\frac{n \left(\frac{\varepsilon}{\varepsilon_{cc}} \right)}{n-1 + \left(\frac{\varepsilon}{\varepsilon_{cc}} \right)^n} \right] \quad 0 < \varepsilon \leq \varepsilon_{cc} \quad (18)$$

$$f'_{cc} = f'_c \left(1.82 - 0.0155 \frac{B_e}{t} \right) \quad f_y < 200 \text{ MPa} \quad (19)$$

$$f'_{cc} = f'_c \left[(-0.0118 f_y + 4.801) - (-0.0002 f_y + 0.0643) \frac{B_e}{t} \right] \quad 200 \text{ MPa} \leq f_y \leq 300 \text{ MPa} \quad (20)$$

$$f'_{cc} = f'_c \left(1.82 - 0.02 \frac{B_e}{t} \right) \quad 300 \text{ MPa} < f_y \leq 500 \text{ MPa} \quad (21)$$

$$f'_{cc} = f'_c \left(1.69 - 0.0172 \frac{B_e}{t} \right) \quad 500 \text{ MPa} < f_y \quad (22)$$

$$\varepsilon_{cc} = \varepsilon_c \left[1 + 5 \left(\frac{f'_{cc}}{f'_c} - 1 \right) \right] \quad (23)$$

$$\varepsilon_c = \begin{cases} 0.002 & f'_{cc} \leq 28 \\ 0.002 + (f'_{cc} - 28) / 54000 & 28 < f'_{cc} \leq 82 \\ 0.003 & f'_{cc} > 82 \end{cases} \quad (24)$$

$$n = [1.02 - 1.17(E_{sec} / E_c)]^{-1.05} \quad (25)$$

$$E_{sec} = \frac{f'_{cc}}{\varepsilon_{cc}} \quad (26)$$

where f_c is the longitudinal compressive stress of the concrete in N/mm^2 , f'_{cc} is the compressive strength of the confined concrete in N/mm^2 , f'_c is the compressive strength of the unconfined concrete in N/mm^2 , f_y is the yield strength of the steel in N/mm^2 , ε is the longitudinal compressive strain of the concrete, ε_{cc} is the strain at f'_{cc} , ε_c is the strain at f'_c , n is the material parameter that depends on the shape of the stress–strain curve, E_{sec} is the secant modulus of elasticity in kN/mm^2 , E_c is the Young's modulus of concrete in kN/mm^2 , and for rectangular section with width B and depth D , the equivalent width $B_e = \sqrt{(B^2 + D^2)}/2$ is used and for square section with width B , $B = B_e$.

The parts AB and BC of the compressive equivalent stress–strain curve for confined concrete represented in Fig. 4 were based on the model given by Susantha *et al.* (2001) and using the proposed confined concrete compressive strength as Eqs. (19) to (22).

5. Verification

5.1 Compressive strength of confined Concrete

The confining effect of steel boxes on concrete is heavily dependent on the concrete compressive strength, steel yield strength, and width-to-thickness ratio. The confining effect of non-compact and slender sections can be negligible when local buckling of steel plates occurs in the elastic region. Nevertheless, the confining effect for compact sections with high strength concrete compressive strength, high strength steel yield strength, and low width-to-thickness ratio can be significant in increasing the concrete crushing strain and therefore it should be considered to accurately calculate the strength of columns (Aslani *et al.* 2015a). In this study, these parameters have been included in the proposed relationship (i.e., Eqs. (19) to (22)).

Fig. 5 shows that the proposed relationship predicts an accurate compressive strength of confined concrete of high strength short square and rectangular CFSTCs. The predictions of compressive strength of confined concrete are also compared with experimental results which are

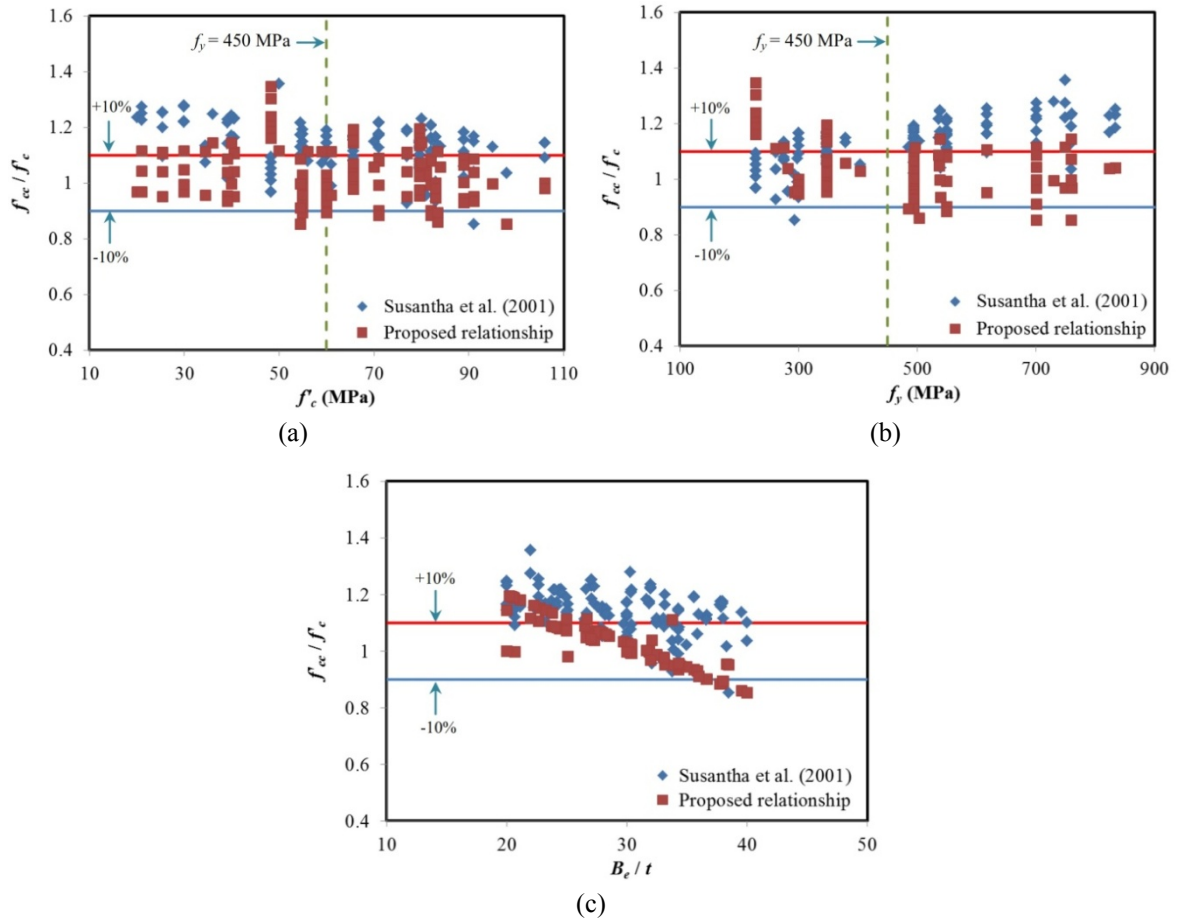


Fig. 5 Ratio maximum compressive strength of confined concrete/compressive strength of unconfined concrete results versus: (a) concrete compressive strength; (b) steel yield strength, and (c) width-to-thickness ratio for short square and rectangular CFSTCs

Table 3 Comparison of results of predicted compressive strength of confined concrete with test results for short square and rectangular CFSTCs

Ref.	S&R-NSS-TC-HSC		S&R-HSS-TC-NSC		S&R-HSS-TC-HSC	
	f_{cc}/f_c		f_{cc}/f_c		f_{cc}/f_c	
	\bar{x}^*	$\bar{\sigma}^*$	\bar{x}	$\bar{\sigma}$	\bar{x}	$\bar{\sigma}$
Susantha <i>et al.</i> (2001)	1.10	0.07	1.20	0.06	1.15	0.06
Proposed relationship	\bar{x}	$\bar{\sigma}$	\bar{x}	$\bar{\sigma}$	\bar{x}	$\bar{\sigma}$
	1.02	0.07	1.00	0.06	0.99	0.05

* \bar{x} = Average and $\bar{\sigma}$ = Standard deviation

categorised into three themes: (a) NSS-TC-HSC; (b) HSS-TC-NSC; and (c) HSS-TC-HSC. Table 3 shows comparisons of the f_{cc}/f_c ratios for the short square and rectangular CFSTCs

experimental results and compressive strength of confined concrete using Susantha *et al.* (2001) and proposed relationships. Table 3 indicates that the proposed relationship provides a better prediction with an average value of f_{cc}/f_c ratios of 1.02, 1.00, and 0.99 compared with the Susantha *et al.* (2001) model for the short square and rectangular NSS-TC-HSC, HSS-TC-NSC, and HSS-TC-HSC, respectively. Furthermore, standard deviations of the ratios of f_{cc}/f_c for the proposed relationship are 0.07, 0.06, and 0.05 for the short square and rectangular NSS-TC-HSC, HSS-TC-NSC, and HSS-TC-HSC, respectively. Fig. 5 and Table 3 demonstrate that the Susantha *et al.* (2001) model is not suitable for high strength concrete compressive strength, high strength steel yield strength, and low width-to-thickness ratios for short square and rectangular CFSTCs.

5.2 Ultimate axial strengths

Table 4 provides details of the material properties, geometry, and test results of short square CFSTCs under axial loading. Test results given by Uy (1998, 2001a), Han (2002), Liu *et al.* (2003), Sakino *et al.* (2004), Mursi and Uy (2004), Liu and Gho (2005), Liu (2005), Han *et al.* (2005), Zhang *et al.* (2005), Lam and Gardner (2008), Lee *et al.* (2009), Chen *et al.* (2011), Zhu *et al.* (2012), Uy *et al.* (2013), and Aslani *et al.* (2015a) were utilised to assess the accuracy of the FEM analysis using Susantha *et al.* (2001) (i.e., Eqs.(4) to (16)) and proposed relationships (i.e., Eqs.(18) to (26)) for short square CFSTCs. It can be seen from Table 4 that the FEM accurately predicts the ultimate axial strengths using proposed relationship for short square CFSTCs. The ratios of the mean ultimate axial strength predicted by the FEM using the Susantha *et al.* (2001) and proposed relationships to the experimental value are 0.89 and 0.98 with the standard deviations of 0.09 and 0.08, respectively.

The predictions of the FEM for the short square CFSTCs are also compared with the categorised: (a) NSS-TC-HSC; (b) HSS-TC-NSC; and (c) HSS-TC-HSC experimental results. Table 5 shows comparisons of the P_{exp}/P_{FEM} ratios for the short square CFSTCs experimental results and FEM predicted ultimate axial loads using the Susantha *et al.* (2001) and proposed relationships.

Table 5 shows that the proposed relationship provides a better prediction with an average value of P_{exp}/P_{FEM} ratios of 0.97, 0.97, and 1.00 compared with the Susantha *et al.* (2001) model for the S-NSS-TC-HSC, S-HSS-TC-NSC, and S-HSS-TC-HSC, respectively. Furthermore, standard deviations of the ratios of P_{exp}/P_{FEM} for the proposed relationship are 0.08, 0.08, and 0.07 for the S-NSS-TC-HSC, S-HSS-TC-NSC, and S-HSS-TC-HSC, respectively. Table 5 demonstrates that the Susantha *et al.* (2001) model is not suitable for high strength short square CFSTCs which average value of P_{exp}/P_{FEM} ratios of 0.90, 0.87, and 0.86 for the S-NSS-TC-HSC, S-HSS-TC-NSC, and S-HSS-TC-HSC, have been achieved respectively.

The comparison of the computed ultimate axial strengths and experimental results for axially loaded short rectangular CFSTCs with concrete confinement effects are provided in Table 6. The experiments conducted by Han (2002), Liu *et al.* (2003), Liu and Gho (2005), Liu (2005), Zhang *et al.* (2005), Lam and Gardner (2008), and Hong *et al.* (2013) are considered for the verification of FEM analysis. It can be observed from Table 6 that the mean values of the computations using the Susantha *et al.* (2001) (i.e., Eqs.(4) to (16)) and proposed relationships (i.e., Eqs.(18) to (26)) to the experimental ultimate axial strengths P_{exp}/P_{FEM} are 0.88 and 1.00 with standard deviations of 0.08 and 0.06, respectively. It appears that the FEM using the proposed relationship can accurately predict the ultimate axial strengths of axially loaded short rectangular CFSTCs with concrete confinement effects.

Table 4 Ultimate axial strengths of axially loaded short square CFSTCs

Specimens	D (mm)	B (mm)	t (mm)	L (mm)	f_y (MPa)	f_c (MPa)	P_{exp} (kN)	P_{exp}/P_{FEM1}^*	P_{exp}/P_{FEM2}^*	Ref.
HSS5	110	110	5	330	750	30	1585	0.78	0.82	Uy (1998)
HSS8	160	160	5	480	750	30	2868	0.87	0.91	
HSS9	160	160	5	480	750	30	2922	0.88	0.93	
HSS12	160	160	5	480	750	30	2242	0.68	0.71	
HSCB1	110	110	5	330	750	50	1940	0.84	0.92	Uy (2001)
HSCB2	110	110	5	330	750	50	2132	0.93	1.00	
rc1-1	100	100	2.86	300	228	48.3	760	1.03	0.97	Han (2002)
rc1-2	100	100	2.86	300	228	48.3	800	1.09	1.02	
rc3-1	100	100	2.86	330	228	48.3	844	1.15	1.06	
rc3-2	100	100	2.86	330	228	48.3	860	1.16	1.09	
C1-1	100.3	98.2	4.18	300	550	71	1490	0.87	0.98	Liu <i>et al.</i> (2003)
C1-2	101.5	100.6	4.18	300	550	71	1535	0.90	1.01	
C2-1	101.2	101.1	4.18	300	550	82	1740	0.94	1.05	
C2-2	100.7	100.4	4.18	300	550	82	1775	0.96	1.08	
CR4-A-2	148	148	4.38	444	262	25.4	1153	0.88	0.94	Sakino <i>et al.</i> (2004)
CR4-A-4-1	148	148	4.38	444	262	40.5	1414	0.88	0.90	
CR4-A-4-2	148	148	4.38	444	262	40.5	1402	0.87	0.89	
CR4-A-8	148	148	4.38	444	262	77	2108	0.93	0.89	
CR6-A-2	144	144	6.36	432	618	25.4	2572	0.90	0.96	
CR6-A-4-1	144	144	6.36	432	618	40.5	2808	0.88	0.94	
CR6-A-4-2	144	144	6.36	432	618	40.5	2765	0.86	0.93	
CR6-A-8	144	144	6.36	432	618	77	3399	0.84	0.92	
CR6-C-2	211	211	6.36	633	618	25.4	3920	0.84	0.94	
CR6-C-4-1	211	211	6.36	633	618	40.5	4428	0.81	0.93	
CR6-C-4-2	211	211	6.36	633	618	40.5	4484	0.83	0.94	
CR6-C-8	211	211	6.36	633	618	77	5758	0.81	0.94	
CR8-C-2	175	175	6.47	525	835	25.4	4210	0.90	0.97	
CR8-C-4-1	175	175	6.47	525	835	40.5	4493	0.86	0.94	
CR8-C-4-2	175	175	6.47	525	835	40.5	4542	0.87	0.95	
CR8-C-8	175	175	6.47	525	835	77	5366	0.83	0.93	
CR4-A-4-3	210	210	5.48	630	294	39.1	3183	1.00	1.11	
CR4-A-9	211	211	5.48	633	294	91.1	4773	0.97	0.99	
CR6-A-4-3	211	211	8.83	633	536	39.1	5898	-	1.08	
CR6-A-9	211	211	8.83	633	536	91.1	7008	-	0.92	
CR6-C-4-3	204	204	5.95	612	540	39.1	4026	0.90	1.04	
CR6-C-9	204	204	5.95	612	540	91.1	5303	0.80	0.93	
CR8-C-4-3	180	180	6.6	540	824	39.1	5028	0.94	1.03	
CR8-C-9	180	180	6.6	540	824	91.1	5873	0.81	0.99	

Table 4 Continued

Specimens	D (mm)	B (mm)	t (mm)	L (mm)	f_y (MPa)	f_c (MPa)	P_{exp} (kN)	P_{exp}/P_{FEM1}^*	P_{exp}/P_{FEM2}^*	Ref.
SH-C160	160	160	5	580	761	20	2831	0.93	1.01	
A9-1	120	120	4	360	495	55	1739	0.94	1.05	
A9-2	120	120	4	360	495	55	1718	0.93	1.04	
A12-1	130	130	4	390	495	55	1963	0.95	1.08	
A12-2	130	130	4	390	495	55	1988	0.96	1.09	
A1	120	120	5.8	360	300	83	1697	0.82	0.96	Liu and Gho (2005)
A2	120	120	5.8	360	300	106	1919	0.81	0.93	
A3-1	200	200	5.8	600	300	83	3996	0.88	0.96	
A3-2	200	200	5.8	600	300	83	3862	0.85	0.93	
R1-1	120	120	4	360	495	60	1701	0.89	1.01	
R1-2	120	120	4	360	495	60	1657	0.87	0.98	
R4-1	130	130	4	390	495	60	2020	0.94	1.06	
R4-2	130	130	4	390	495	60	2018	0.94	1.06	
R7-1	106	106	4	320	495	89	1749	0.92	0.99	Liu (2005)
R8-1	106	106	4	390	495	89	1752	0.91	0.99	
R10-1	140	140	4	420	495	89	2752	0.94	1.08	
R10-2	140	140	4	420	495	89	2828	0.97	1.11	
SA1-1	60	60	1.87	180	282	81	382	0.94	1.00	
SA1-2	60	60	1.87	180	282	81	350	0.86	0.91	Han <i>et al.</i> (2005)
SC1-1	60	60	2	180	404	81	422	0.85	0.95	
SC1-2	60	60	2	180	404	81	406	0.82	0.92	
4	101.3	101.3	4.97	303.9	347.3	65.6	1310	0.92	0.96	
5	103.6	103.6	4.9	310.8	347.3	65.6	1340	0.94	0.98	
6	102	102	4.97	306	347.3	65.6	1370	0.96	1.00	
7	142	142	5.11	426	347.3	65.6	2160	0.90	0.97	Zhang <i>et al.</i> (2005)
8	142	142	5.08	426	347.3	65.6	2250	0.93	1.01	
9	141.4	141.4	5.07	424.2	347.3	65.6	2280	0.95	1.03	
13	103.5	103.5	5.01	310.5	347.3	79.6	1500	0.94	0.98	
14	102.1	102.1	4.97	306.3	347.3	79.6	1330	0.84	0.87	Lam and Gardner (2008)
15	101.9	101.9	5.03	305.7	347.3	79.6	1440	0.91	0.94	
16	142.3	142.3	5.09	426.9	347.3	79.6	2520	0.95	1.02	
17	142.4	142.4	5.1	427.2	347.3	79.6	2610	0.99	1.06	
18	139.1	139.1	5.06	417.3	347.3	79.6	1700	0.64	0.69	
SHS150×150× 6-C80	150	150	6	300	497	83.5	3020	0.79	0.87	
NCFT160R	160	160	8	480	539	40	3449	-	0.94	Lee <i>et al.</i> (2009)
NCFT240R	240	240	8	720	539	40	6009	-	0.99	

Table 4 Continued

Specimens	D (mm)	B (mm)	t (mm)	L (mm)	f_y (MPa)	f_c (MPa)	P_{exp} (kN)	P_{exp}/P_{FEM1}^*	P_{exp}/P_{FEM2}^*	Ref.
L0	120	120	3.5	400	298	34.4	863	0.83	0.94	Chen <i>et al.</i> (2011)
H0	120	120	3.5	400	298	61	1354	0.98	1.09	
L0	120	120	4.5	400	275	34.4	1088	0.95	1.02	
H0	120	120	4.5	400	275	61	1469	0.97	1.02	
Pa-6-2	166	164	6.2	601	537	30	3010	0.96	1.04	
CB20 - SH (A)	100	100	5	350	760	80	2524	1.05	1.12	Uy <i>et al.</i> (2013)
CB20 - SH (B)	100	100	5	350	760	80	2632	1.10	1.18	
CB 25 - SH (A)	125	125	5	437.5	760	80	3024	0.91	1.02	
CB 25 - SH (B)	125	125	5	437.5	760	80	2971	0.89	1.01	
CB 30 - SH (A)	150	150	5	525	760	95	4115	0.88	1.02	
CB 30 - SH (B)	150	150	5	525	760	95	3968	0.85	0.99	
CB 40 - SH (A)	200	200	5	700	760	98	5184	0.72	0.89	
CB40SH (B)	200	200	5	700	760	98	5604	0.78	0.96	
SC2B	110	110	5	300	701	21	1934	1.06	1.12	Aslani <i>et al.</i> (2015a)
SC3B	135	135	5	375	701	21	2348	1.01	1.08	
SC4B	160	160	5	450	701	21	2828	0.98	1.08	
HSSC1	120	120	5	330	701	54.5	2203	0.86	0.93	
HSSC2	120	120	5	330	701	54.5	2234	0.87	0.95	
HSSC3	150	150	5	420	701	54.5	2942	0.83	0.95	
HSSC4	150	150	5	420	701	54.5	2840	0.81	0.92	
HSSC5	180	180	5	510	701	54.5	3118	0.68	0.81	
HSSC6	180	180	5	510	701	54.5	3243	0.71	0.85	
HSSC7	200	200	5	570	701	54.5	3882	0.74	0.91	
HSSC8	200	200	5	570	701	54.5	3856	0.73	0.90	
Mean								0.89	0.98	
Standard Deviation (SD)								0.09	0.08	

* P_{FEM1} and P_{FEM2} are FE predicted ultimate axial strengths using Susantha *et al.* (2001) and proposed relationships

Three available categorised experimental results for short rectangular CFSTCs (i.e., NSS-TC-HSC, HSS-TC-NSC, and HSS-TC-HSC) are compared with predictions of FEM, as shown in Table 5. Table 5 displays comparisons of the P_{exp}/P_{FEM} ratios for the short rectangular CFSTCs experimental results and FEM predicted ultimate axial loads using the Susantha *et al.* (2001) and proposed relationships. Table 5 indicates that the proposed relationship provides a better prediction with an average value of P_{exp}/P_{FEM} ratios of 0.99, 1.01, and 1.00 compared with the Susantha *et al.* (2001) model for the R-NSS-TC-HSC, R-HSS-TC-NSC, and R-HSS-TC-HSC, respectively. Furthermore, standard deviations of the ratios of P_{exp}/P_{FEM} for the proposed relationship are 0.05, 0.05, and 0.05 for the R-NSS-TC-HSC, R-HSS-TC-NSC, and R-HSS-TC-HSC, respectively. Also, Table 5 illustrates that the Susantha *et al.* (2001) model is not suitable for high strength short rectangular CFSTCs.

Table 5 Comparison of results of FE predicted ultimate axial strengths with test results for short rectangular CFSTCs

Ref.	S-NSS-TC-HSC		S-HSS-TC-NSC		S-HSS-TC-HSC	
	P_{exp}/P_{FEM}		P_{exp}/P_{FEM}		P_{exp}/P_{FEM}	
	\bar{x}^*	$\bar{\sigma}^*$	\bar{x}	$\bar{\sigma}$	\bar{x}	$\bar{\sigma}$
Susantha <i>et al.</i> (2001)	0.90	0.08	0.87	0.09	0.86	0.08
Proposed relationship	\bar{x}	$\bar{\sigma}$	\bar{x}	$\bar{\sigma}$	\bar{x}	$\bar{\sigma}$
	0.97	0.08	0.97	0.08	1.00	0.07
Ref.	R-NSS-TC-HSC		R-HSS-TC-NSC		R-HSS-TC-HSC	
	P_{exp}/P_{FEM}		P_{exp}/P_{FEM}		P_{exp}/P_{FEM}	
	\bar{x}	$\bar{\sigma}$	\bar{x}	$\bar{\sigma}$	\bar{x}	$\bar{\sigma}$
Susantha <i>et al.</i> (2001)	0.87	0.05	0.90	0.06	0.84	0.05
Proposed relationship	\bar{x}	$\bar{\sigma}$	\bar{x}	$\bar{\sigma}$	\bar{x}	$\bar{\sigma}$
	0.99	0.05	1.01	0.05	1.00	0.05

5.3 Axial load-strain curves

The axial load-strain curves provide important information on the ultimate axial strengths, initial stiffness, ductility, strain hardening and strain softening of short CFSTCs under axial loading. The accuracy of the FEM is examined by comparing the experimental results and numerical predictions.

The FEM was utilised to predict the axial load-strain curves of short square and rectangular CFSTCs tested by Han *et al.* (2005), Liu (2005), Uy (2001b), and Liu *et al.* (2003). Figs. 6 to 9 compare the predictions of axial load-strain curves with the experimental results for short square and rectangular CFSTCs. It can be seen from Figs. 6 to 9 that the axial load-strain curve predicted by FEM using the proposed relationship agrees reasonably well with the experimental results. The initial stiffness and post-peak of the axial load-strain curves predicted by the FEM is in good agreement with the Han *et al.* (2005) and Uy (2001b)'s experimental results. The FEM tends to accurately predict the ultimate axial strength for tested short square and rectangular CFSTCs. However, the experimental curve slightly departs from the computational one after the ultimate axial strength for Liu (2005) and Liu *et al.* (2003)'s experimental results.

Table 6 Ultimate axial strengths of axially loaded short rectangular CFSTCs

Specimens	D (mm)	B (mm)	t (mm)	L (mm)	f_y (MPa)	f_c (MPa)	P_{exp} (kN)	P_{exp}/P_{FEM1}	P_{exp}/P_{FEM2}	Ref.
rc5-1	90	70	2.86	270	228	48.3	554	1.04	0.99	
rc5-2	90	70	2.86	270	228	48.3	576	1.08	1.03	
rc6-1	100	75	2.86	300	228	48.3	640	1.04	1.00	Han (2002)
rc6-2	100	75	2.86	300	228	48.3	672	1.10	1.04	
rc7-1	120	90	2.86	360	228	48.3	800	0.98	0.96	
rc7-2	120	90	2.86	360	228	48.3	760	0.93	0.91	

Table 6 Ultimate axial strengths of axially loaded short rectangular CFSTCs

Specimens	D (mm)	B (mm)	t (mm)	L (mm)	f_y (MPa)	f_c (MPa)	P_{exp} (kN)	P_{exp}/P_{FEM1}	P_{exp}/P_{FEM2}	Ref.
rc11-1	130	85	2.86	390	228	48.3	760	0.92	0.89	Han (2002)
rc11-2	130	85	2.86	390	228	48.3	820	0.99	0.97	
rc12-1	140	80	2.86	420	228	48.3	880	1.04	1.27	
rc12-2	140	80	2.86	420	228	48.3	740	0.88	1.06	
C5-1	120.7	80.1	4.18	360	550	71	1450	0.85	0.97	Liu <i>et al.</i> (2003)
C5-2	119.3	80.6	4.18	360	550	71	1425	0.84	0.95	
C6-1	119.6	80.6	4.18	360	550	82	1560	0.86	0.98	
C6-2	120.5	80.6	4.18	360	550	82	1700	0.93	1.06	
C7-1	179.7	121.5	4.18	540	550	71	2530	0.80	0.98	
C8-1	180.4	119.8	4.18	540	550	82	2970	0.88	1.08	
C8-2	179.2	121.3	4.18	540	550	82	2590	0.76	0.93	
C9-1	160.2	81.4	4.18	480	550	71	1710	0.79	0.93	
C9-2	160.7	80.5	4.18	480	550	71	1820	0.84	0.98	
C10-1	160.1	81	4.18	480	550	82	1880	0.81	0.95	
C10-2	160.6	80.1	4.18	480	550	82	2100	0.91	1.06	
C11-1	199.8	101.2	4.18	600	550	71	2350	0.79	0.97	
C11-2	200.2	98.9	4.18	600	550	71	2380	0.80	0.98	
C12-1	199.2	102.1	4.18	600	550	82	2900	0.89	1.11	
C12-2	199.8	99.6	4.18	600	550	82	2800	0.86	1.08	
A10-1	150	100	4	450	495	55	1815	0.93	1.08	Liu and Gho (2005)
A10-2	150	100	4	450	495	55	1763	0.91	1.04	
A11-1	180	90	4	540	495	55	1725	0.82	0.98	
A11-2	180	90	4	540	495	55	1742	0.83	0.99	
A13-1	160	110	4	480	495	55	1947	0.89	1.04	
A13-2	160	110	4	480	495	55	1912	0.88	1.03	
A14-1	190	100	4	570	495	55	2035	0.87	1.05	
A14-2	190	100	4	570	495	55	2138	0.91	1.11	
A4-1	130	100	5.8	390	300	83	1601	0.83	0.92	
A4-2	130	100	5.8	390	300	83	1566	0.81	0.90	
A5-1	130	100	5.8	390	300	106	1854	0.83	0.99	
A5-2	130	100	5.8	390	300	106	1779	0.80	0.94	
A6-1	220	170	5.8	660	300	83	3684	0.81	0.93	
A6-2	220	170	5.8	660	300	83	3717	0.82	0.94	
A7-1	180	100	5.8	540	300	83	2059	0.79	0.96	
A7-2	180	100	5.8	540	300	83	2019	0.78	0.94	
A8-1	180	100	5.8	540	300	106	2287	0.76	0.92	
A8-2	180	100	5.8	540	300	106	2291	0.76	0.93	

Table 6 Continued

Specimens	D (mm)	B (mm)	t (mm)	L (mm)	f_y (MPa)	f_c (MPa)	P_{exp} (kN)	P_{exp}/P_{FEM1}	P_{exp}/P_{FEM2}	Ref.
R2-1	150	100	4	450	495	60	1735	0.85	0.99	
R2-2	150	100	4	450	495	60	1778	0.88	1.02	
R3-1	180	90	4	540	495	60	1773	0.81	0.97	
R3-2	180	90	4	540	495	60	1795	0.82	0.98	
R5-1	160	110	4	480	495	60	1982	0.87	1.02	
R5-2	160	110	4	480	495	60	1923	0.84	0.99	
R6-1	190	100	4	570	495	60	2049	0.83	1.02	
R6-2	190	100	4	570	495	60	2124	0.87	1.06	Liu (2005)
R7-2	130	90	4	320	495	89	1824	0.90	1.01	
R8-2	160	80	4	390	495	89	1806	0.81	0.95	
R9-1	130	90	4	480	495	89	1878	0.92	1.03	
R9-2	160	80	4	480	495	89	1858	0.83	0.97	
R11-1	160	125	4	480	495	89	2580	0.85	1.00	
R11-2	160	125	4	480	495	89	2674	0.88	1.03	
25	159.1	103.3	4.8	477.3	347.3	65.6	1875	0.91	1.02	
26	156.7	102.4	4.8	470.1	347.3	65.6	1915	0.93	1.04	
27	158.8	104.4	4.85	476.4	347.3	65.6	1820	0.88	0.99	
28	130.3	101.6	5.03	390.9	347.3	65.6	1580	0.88	0.94	Zhang <i>et al.</i> (2005)
29	130.3	102.3	5.14	390.9	347.3	65.6	1600	0.89	0.96	
30	130.3	102.3	5.14	390.9	347.3	65.6	1640	0.92	0.98	
31	167.4	136	5.13	502.2	347.3	65.6	2510	0.93	1.04	
32	170.8	135.3	5.07	512.4	347.3	65.6	2470	0.91	1.02	
33	188.4	121.6	4.88	565.2	347.3	65.6	2260	0.83	0.97	
34	190.9	120.4	4.83	572.7	347.3	65.6	2510	0.93	1.09	
41	125.7	102.7	5.15	377.1	347.3	79.6	1840	0.94	1.02	
42	130	102.4	5.03	390	347.3	79.6	1820	0.93	1.01	
43	132.3	102.7	4.98	396.9	347.3	79.6	1725	0.88	0.95	
44	156.9	103.4	4.71	470.7	347.3	79.6	2090	0.90	1.01	Zhang <i>et al.</i> (2005)
45	162	106.9	4.81	486	347.3	79.6	2320	1.00	1.12	
46	158.9	102.6	4.74	476.7	347.3	79.6	2060	0.88	1.00	
47	167.9	137.1	5.1	503.7	347.3	79.6	2600	0.85	0.96	
48	172.7	133.2	5.08	518.1	347.3	79.6	2700	0.89	1.00	
49	194.8	121	4.72	584.4	347.3	79.6	2700	0.88	1.02	
50	189.6	121.7	4.81	568.8	347.3	79.6	2680	0.88	1.01	
RHS200× 110×4 – C80	200	100	4	300	503	83.5	2180	0.68	0.86	Lam and Gardner (2008)
RHS140× 80×3 – C80	140	80	3	300	486	83.5	1259	0.75	0.93	

Table 6 Continued

Specimens	D (mm)	B (mm)	t (mm)	L (mm)	f_y (MPa)	f_c (MPa)	P_{exp} (kN)	P_{exp}/P_{FEM1}	P_{exp}/P_{FEM2}	Ref.
RAC-36-30	230	115	6	690	730	30	4017	1.02	1.12	Hong <i>et al.</i> (2013)
Mean					0.88		1.00			
Standard deviation (SD)					0.08		0.06			

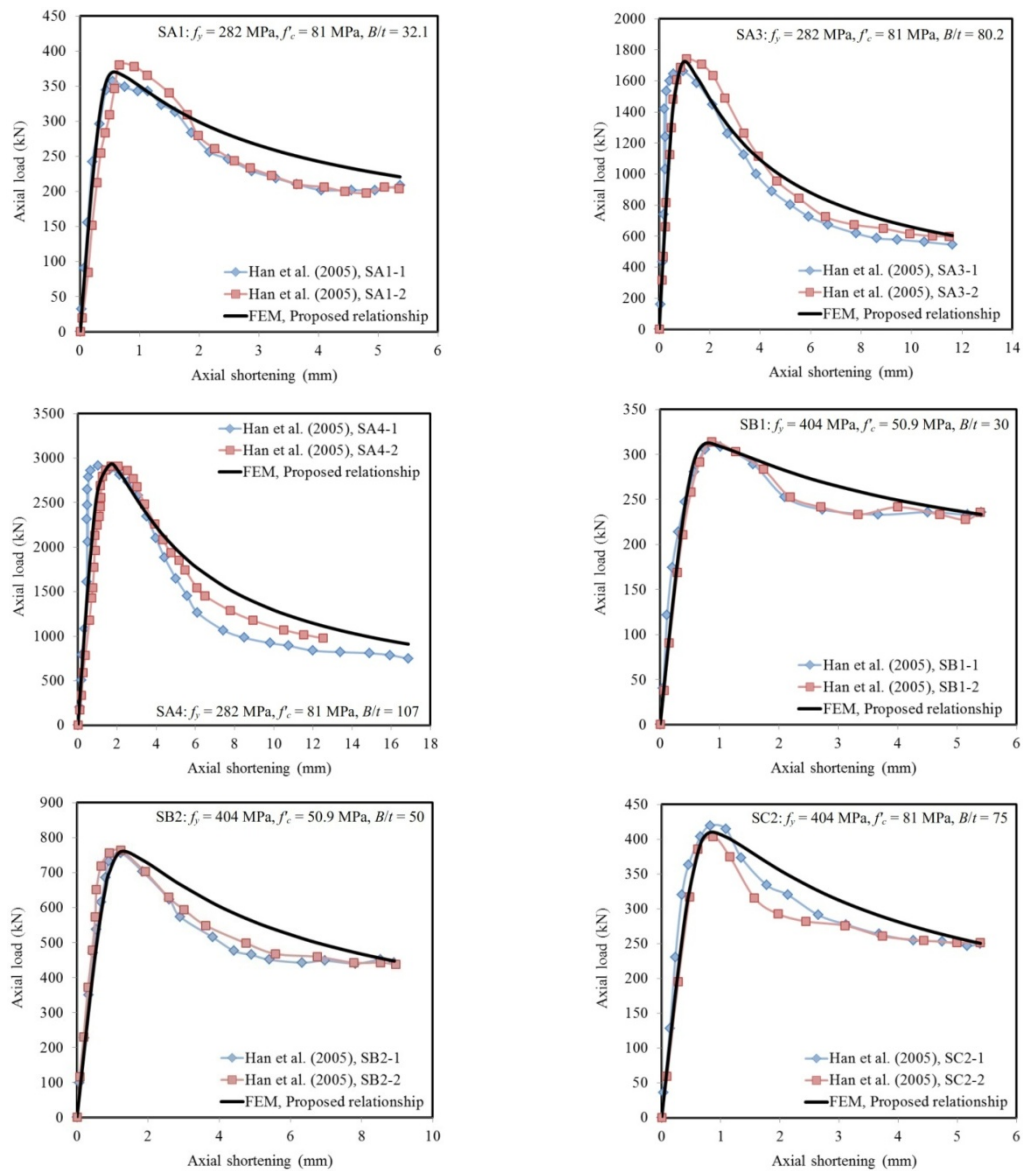


Fig. 6 Comparisons of predicted and Han *et al.*'s (2005) experimental axial load-strain curves for short square and rectangular CFSTCs under axial compression

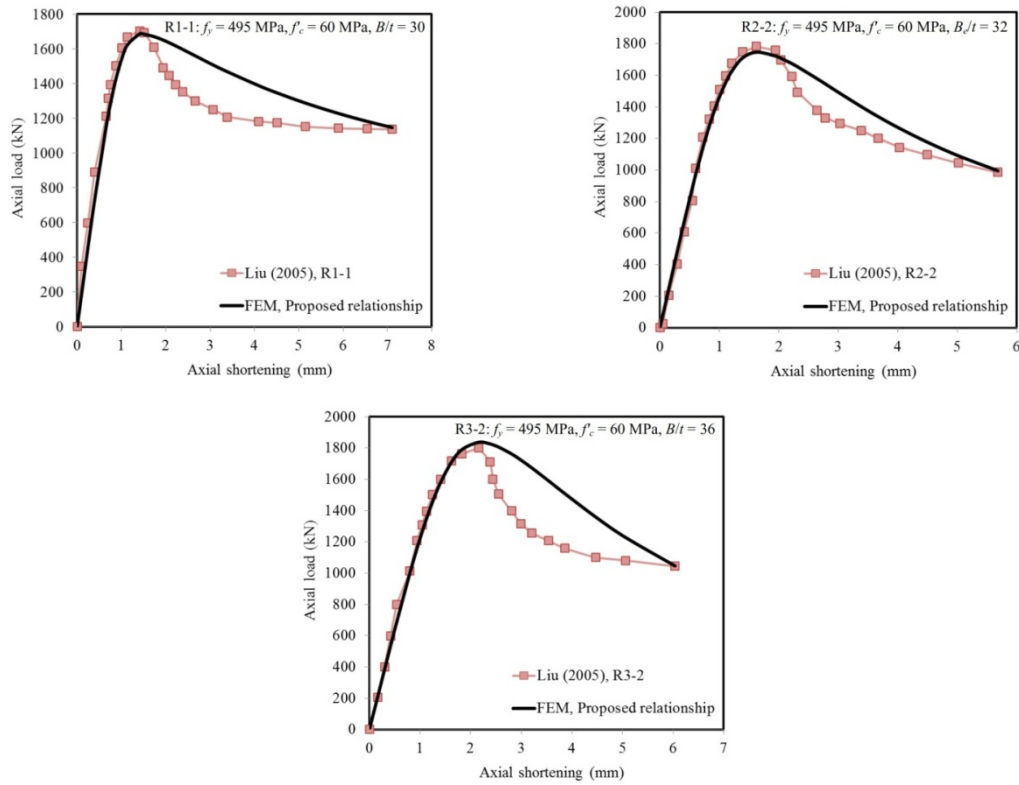


Fig. 7 Comparisons of predicted and Liu's (2005) experimental axial load-strain curves for short square and rectangular CFSTCs under axial compression

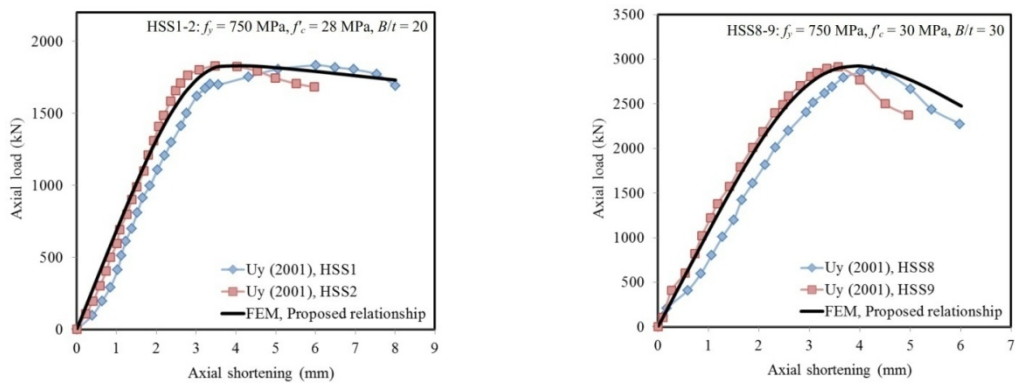


Fig. 8 Comparisons of predicted and Uy's (2001a) experimental axial load-strain curves for short square CFSTCs under axial compression

6. Parametric studies

The behaviour of axially loaded short CFSTCs is affected by concrete compressive strength, steel yield strength and width-to-thickness ratio. The FEM using the Susantha *et al.* (2001) and

proposed relationships is utilised for examining the effects of concrete compressive strength, steel yield strength, and width-to-thickness ratio on the behaviour of short square and rectangular CFSTCs under axial loading. The FEM typical failure modes for short square and rectangular CFSTCs under axial loading are depicted in Fig. 10.

6.1 Influence of concrete compressive strength

The influence of concrete compressive strength on the predicted behaviour of short square and rectangular CFSTCs was investigated herein. The ultimate axial strength of axially loaded CFST short columns increases with an increase in the concrete compressive strength regardless of the cross-sectional shape, as illustrated in Figs. 6 to 9. As an example for short square CFSTCs with $f_y = 618 \text{ N/mm}^2$ and $B/t = 33$ from Sakino *et al.* (2004), an increase in the concrete compressive strength from 25.4 N/mm^2 to 40.5 N/mm^2 and 77 N/mm^2 , the ultimate axial strength is increased by 14% and 47%, respectively. Also, as an example for rectangular CFSTCs with $f_y = 495 \text{ N/mm}^2$ and $B_e/t = 35$ from Liu (2005), an increase in the concrete compressive strength from 60 N/mm^2 to 89 N/mm^2 , the ultimate axial strength is increased by 35%.

Fig. 11 indicates comparisons of experimental results to predicted FEM results using the Susantha *et al.* (2001) and proposed relationships versus concrete compressive strength for short square and rectangular CFSTCs. Fig. 11 shows that the proposed relationship provides a better

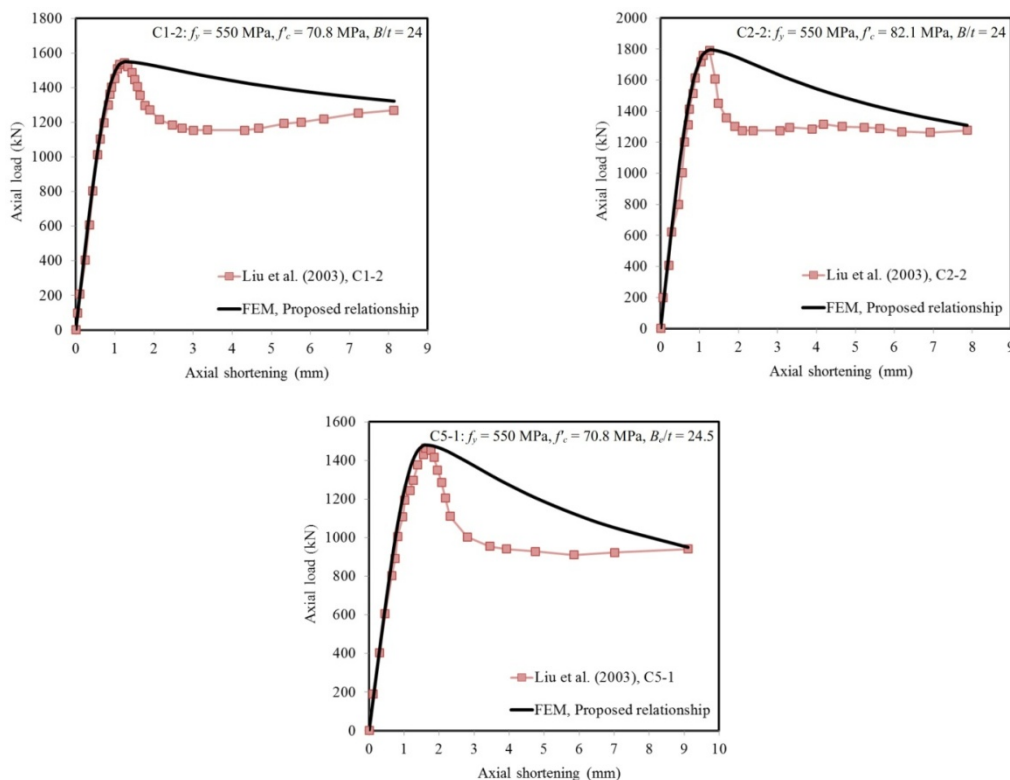


Fig. 9 Comparisons of predicted and Liu *et al.*'s (2003) experimental axial load-strain curves for short square and rectangular CFSTCs under axial compression

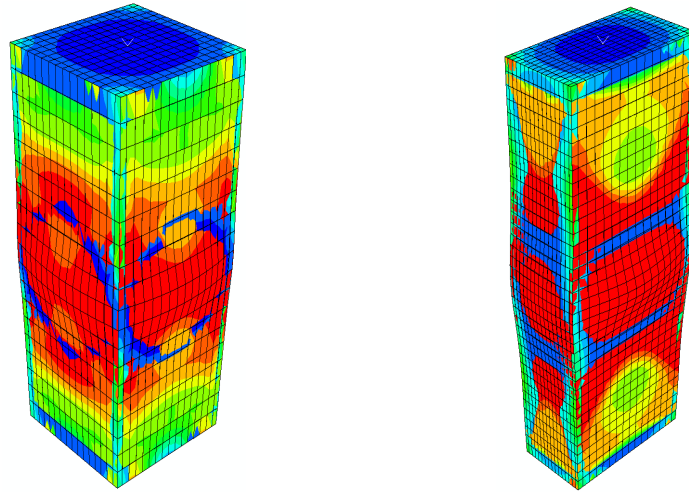


Fig. 10 Typical failure modes for short square and rectangular CFSTCs under axial loading

prediction versus the concrete compressive strength in the range of normal to high strength compared with the Susantha *et al.* (2001) model.

However, the Susantha *et al.* (2001) model is inaccurate in predicting the behaviour of short square and rectangular CFSTCs with high strength concrete. Susantha *et al.* (2001) model's prediction insufficiency is obvious for short rectangular CFSTCs with high strength concrete, as shown in Fig. 11(b).

6.2 Influence of steel yield strength

The strength and ductility of CFSTCs is significantly influenced by the yield strength of the encased steel tube regardless of the sectional shape. Fig. 12 depicts the influence of the steel yield strength on the behaviour of short square and rectangular CFSTCs under axial loading.

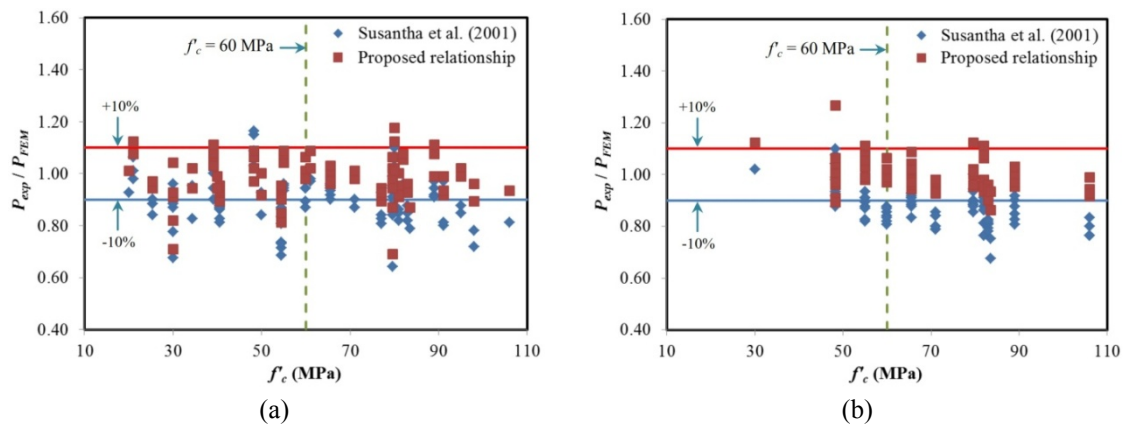


Fig. 11 Ratio experimental results/FEM predicted results versus concrete compressive strength for: (a) short square; and (b) short rectangular CFSTCs

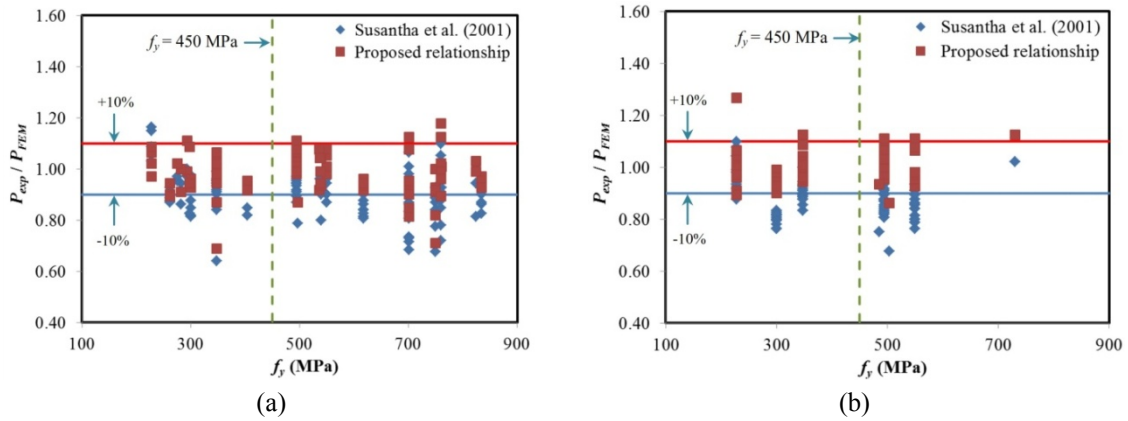


Fig. 12 Ratio experimental results/FEM predicted results versus steel yield strength for: (a) short square; and (b) short rectangular CFSTCs

It can be observed from Figs. 6 to 9 that the initial axial stiffness of CFSTCs is not affected by the steel yield strength regardless of the sectional shape. In contrast, the ultimate axial strength is significantly affected by the steel yield strength. It was found that the ductility of CFSTCs decreases with an increase in the steel yield strength. This is because of the reduced ductility of high strength steel. An increase in the steel yield strength considerably increases the ultimate axial strength of a CFSTC.

As an example for short square CFSTCs with $f_c = 91.1 \text{ N/mm}^2$ and $B/t = 27\text{-}38$ from Sakino *et al.* (2004), an increase in the steel yield strength from 294 N/mm^2 to 540 N/mm^2 and 824 N/mm^2 , the ultimate axial strength is increased by 11% and 23%, respectively. Also, for rectangular CFSTCs with $f_c = 83\text{-}89 \text{ N/mm}^2$ and $B_e/t = 20\text{-}27$ from Liu (2005) and Liu and Gho (2005), an increase in the steel yield strength from 300 N/mm^2 to 495 N/mm^2 , an ultimate axial strength increase of 15% is observed.

Fig. 12 shows comparisons of experimental results to predicted FEM results using the Susantha *et al.* (2001) and proposed relationships versus steel yield strength for short square and rectangular CFSTCs. Fig. 12 shows that the proposed relationship provides a better prediction versus the steel yield strength in the range of normal to high strength compared with the Susantha *et al.* (2001) model. Conversely, the Susantha *et al.* (2001) model does not adequately predict the behaviour of short square and rectangular CFSTCs especially with high strength concrete and steel.

6.3 Influence of width-to-thickness (B/t) ratio

The width-to-thickness ratio of compact plates is one of the parameters significantly affecting the concrete confinement offered by the encased steel tube regardless of the sectional shape. The steel contribution to ultimate axial strength in CFSTCs is also affected by the width-to-thickness ratio. This is due mainly to the steel area varying with the width-to-thickness ratio. The width-to-thickness ratio was considered by varying the thickness of the steel tube while maintaining the same cross-section size.

The influence of width-to-thickness ratio on the axial load-strain curves for short square and rectangular CFSTCs is presented in Fig. 6 to 9. Also, Fig. 13 depicts the influence of width-to-thickness ratio on the behaviour of short square and rectangular CFSTCs under axial loading. It

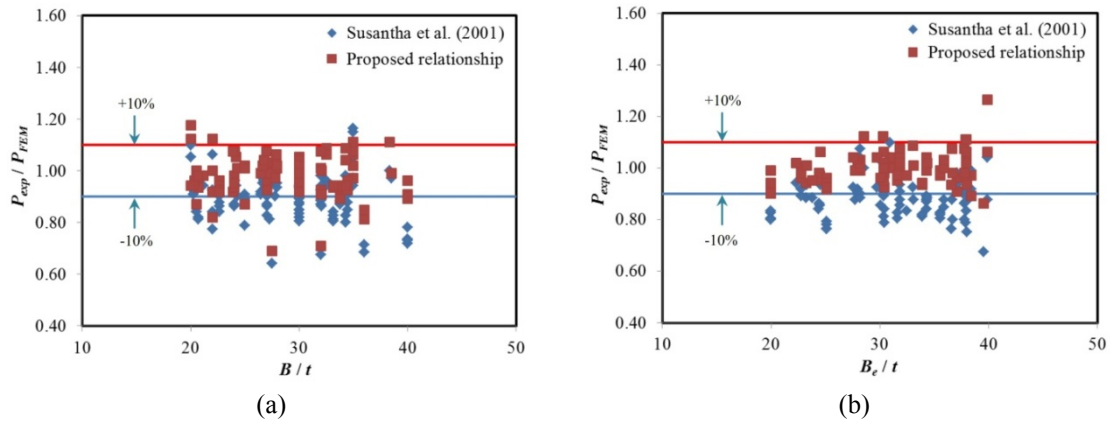


Fig. 13 Ratio experimental results/FEM predicted results versus width-to-thickness ratio for: (a) short square; and (b) short rectangular CFSTCs

can clearly be seen from Tables 4 and 6 that by increasing the width-to-thickness ratio decreases the ultimate axial strength regardless of the sectional shape. It should be noted that by reducing the width-to-thickness ratio increases the steel area for the column cross-section.

As an instance for short square CFSTCs with $f_y = 701 \text{ N/mm}^2$ and $f_c = 54.5 \text{ N/mm}^2$ from Aslani *et al.* (2015a), an increase in the width-to-thickness ratio from 24 to 30, 36, and 40, the ultimate axial strength is increased by 30%, 43%, and 74%, respectively. Also, as an instance for rectangular CFSTCs with $f_y = 550 \text{ N/mm}^2$ and $f_c = 82 \text{ N/mm}^2$ from Liu *et al.* (2003), an increase in the width-to-thickness ratio from 24 to 30, and 37, the ultimate axial strength is increased by 22%, and 71%, respectively.

Fig. 13 displays comparisons of the experimental results to FEM predicted results using Susantha *et al.*'s (2001) and proposed relationships versus width-to-thickness ratio for short square and rectangular CFSTCs. Fig. 13 shows that the proposed relationship provides a better prediction versus width-to-thickness ratio in the range of low to high compared with the Susantha *et al.* (2001) model. On the contrary, the Susantha *et al.* (2001) model does not provide suitable prediction for short square and rectangular CFSTCs with higher width-to-thickness ratio. The Susantha *et al.* (2001) model prediction deficiency is clearer for short rectangular CFSTCs with higher width-to-thickness ratio, as shown in Fig. 13(b).

7. Design recommendations

7.1 AS 5100.6 (2004)

The ultimate axial strengths of short square and rectangular CFSTCs under axial compression are calculated by utilising the design equations given in AS 5100.6 (2004). Maximum yield strength of steel is limited up to 350 N/mm^2 in AS 5100.6 (2004) for the design of an axially loaded CFSTC. The steel contribution factor for the CFSTCs is constrained between 0.2 and 0.9. The ultimate axial strength of an axially loaded CFSTC can be calculated as follows

$$P_{u,AS5100.6} = \alpha_c (A_s f_y + A_c f'_c) \quad (27)$$

$$\alpha_c = \xi \left[1 - \sqrt{1 - \left(\frac{90}{\xi \lambda} \right)^2} \right] \quad (28)$$

$$\xi = \frac{\left(\frac{\lambda}{90} \right)^2 + 1 + \eta}{2 \left(\frac{\lambda}{90} \right)^2} \quad (29)$$

$$\lambda = \lambda_\eta + \alpha_a \alpha_b \quad (30)$$

$$\eta = 0.00326 (\lambda_\eta - 13.5) \geq 0 \quad (31)$$

$$\lambda_\eta = \left(\frac{L_e}{r} \right) \sqrt{k_f \left(\frac{f_y}{250} \right)} \quad (32)$$

$$\alpha_a = \frac{2100 (\lambda_\eta - 13.5)}{\lambda_\eta^2 - 15.3 \lambda_\eta + 2050} \quad (33)$$

$$L_e = k_e L \quad (34)$$

where A_s is the cross-section area of steel tube, A_c is the cross-sectional area of the concrete core, α_c is the compression member slenderness reduction factor, ξ is the compression member factor, α_b is the appropriate section constant give in AS5100.6 (2004) Tables 10.3.3(A&B), k_f is the form factor, L_e is the effective length, and k_e is the member effective length factor.

7.2 Eurocode 4 (2004)

The design recommendations given in Eurocode 4 (2004) take into account the effect of concrete confinement offered by the encased steel tube. The design equation is given as

$$P_{u,EC4} = A_s f_y + A_c f'_c \quad (35)$$

in which $B / t \leq 52 \sqrt{235 / f_y}$.

7.3 Proposed design model

The ultimate axial strength of short square and rectangular CFSTCs subjected to axial compression depends on the material and geometric properties. It also relies on the concrete confinement offered by the encased steel tube. A design equation is proposed using Eqs. (19) to (22) and nonlinear regression analysis for predicting the ultimate axial strength of axially loaded short square and rectangular CFSTCs. The proposed design equation is given as follows

$$P_{u.sqr} = A_s f_y + 0.82 A_c f'_{cc} \quad (36)$$

$$P_{u.rec} = A_s f_y + 0.85 A_c f'_{cc} \quad (37)$$

in which f'_{cc} is calculated by Eqs. (19) to (22).

7.4 Evaluation of design equations

A generic design model is developed herein for determining the ultimate axial strengths of short square and rectangular CFSTCs under axial loading. The material, geometric parameters, and comparison of ultimate axial strengths of short square and rectangular CFSTCs determined by experiment, design codes and proposed design model are provided in Tables 7-9 and Figs. 14-15, respectively.

It can be seen from Fig. 14 and Table 7 that the proposed design model accurately predicts the ultimate axial strengths of short square CFSTCs. The ratios of the mean ultimate axial strength predicted by the proposed design model, AS5100.6 (2004), and Eurocode 4 (2004) to the experimental values are 1.00, 1.01, and 1.07 with a standard deviation of 0.08, 0.10, and 0.11, respectively.

The predictions of design codes and proposed design model for the short square CFSTCs are also compared with the categorised experimental results into the three available themes: (a) NSS-TC-HSC; (b) HSS-TC-NSC; and (c) HSS-TC-HSC. Table 8 shows comparisons of the P_{exp}/P_{cal} ratios for the short square CFSTCs experimental results and predicted ultimate axial loads using design codes and proposed design model.

Table 8 shows that the proposed design model provides a better prediction with an average value of P_{exp}/P_{cal} ratios of 1.00, 0.99, and 1.01 compared with the AS5100.6 (2004) and Eurocode 4 (2004) for the S-NSS-TC-HSC, S-HSS-TC-NSC, and S-HSS-TC-HSC, respectively. Furthermore, standard deviations of the ratios of P_{exp}/P_{cal} for the proposed design model are 0.07, 0.08, and 0.07 for the S-NSS-TC-HSC, S-HSS-TC-NSC, and S-HSS-TC-HSC, respectively. Also, it can be seen that the design codes, AS 5100.6 (2004) and Eurocode 4 (2004) provide conservative predictions of the ultimate axial strengths of short square CFSTCs.

The comparison of the design codes and proposed design models predicted ultimate axial strengths and experimental results for axially loaded short rectangular CFSTCs with concrete confinement effects given in Fig. 15 and Table 9. It can be observed from Table 9 that the mean values of the computations using the proposed design model, AS5100.6 (2004), and Eurocode 4 (2004) to the experimental ultimate axial strengths P_{exp}/P_{cal} are 1.00, 1.02, and 1.10 with standard deviations of 0.05, 0.08, and 0.09, respectively. It appears that the proposed design model can accurately predict the ultimate axial strengths of axially loaded short rectangular CFSTCs with concrete confinement effects.

Three available categorised experimental results themes: (a) NSS-TC-HSC; (b) HSS-TC-NSC; and (c) HSS-TC-HSC for short rectangular CFSTCs are compared with the predictions of the design codes and proposed design model, as shown in Table 8. Table 8 shows comparisons of the P_{exp}/P_{cal} ratios for the short rectangular CFSTCs experimental results and predicted ultimate axial loads.

Table 8 indicates that the proposed design model provides a better prediction with an average value of P_{exp}/P_{cal} ratios of 1.00, 1.01, and 1.00 compared with the AS5100.6 (2004) and Eurocode

4 (2004) for the R-NSS-TC-HSC, R-HSS-TC-NSC, and R-HSS-TC-HSC, respectively. Furthermore, standard deviations of the ratios of P_{exp}/P_{cal} for the proposed design model are 0.05, 0.04, and 0.04 for the R-NSS-TC-HSC, R-HSS-TC-NSC, and R-HSS-TC-HSC, respectively.

Table 7 Comparison of ultimate axial strengths of square CFSTCs determined by experiment, design codes and proposed design model

Specimens	P_{exp} (kN)	$P_{exp}/P_{u.sqr}$	$P_{exp}/P_{u.AS5100.6}$	$P_{exp}/P_{u.EC4}$	Ref.	
HSS5	1585	0.84	0.85	0.87	Uy (1998)	
HSS8	2868	0.97	0.96	0.99		
HSS9	2922	0.99	0.97	1.01		
HSS12	2242	0.76	0.75	0.77		
HSCB1	1940	0.92	0.94	0.97	Uy (2001a)	
HSCB2	2132	1.01	1.03	1.07		
rc1-1	760	0.99	1.11	1.23	Han (2002)	
rc1-2	800	1.04	1.17	1.29		
rc3-1	844	1.10	1.24	1.37		
rc3-2	860	1.12	1.26	1.39		
C1-1	1490	1.00	1.02	1.09	Liu <i>et al.</i> (2003)	
C1-2	1535	1.01	1.02	1.09		
C2-1	1740	1.07	1.09	1.17		
C2-2	1775	1.10	1.12	1.20		
CR4-A-2	1153	0.97	1.00	1.07	Sakino <i>et al.</i> (2004)	
CR4-A-4-1	1414	0.94	0.98	1.07		
CR4-A-4-2	1402	0.93	0.97	1.06		
CR4-A-8	2108	0.93	0.98	1.09		
CR6-A-2	2572	0.98	0.99	1.01		
CR6-A-4-1	2808	0.97	0.98	1.02		
CR6-A-4-2	2765	0.95	0.97	1.00		
CR6-A-8	3399	0.95	0.97	1.03		
CR6-C-2	3920	0.95	0.93	0.96		
CR6-C-4-1	4428	0.95	0.92	0.97		
CR6-C-4-2	4484	0.96	0.93	0.98		
CR6-C-8	5758	0.96	0.92	0.99		
CR8-C-2	4210	0.98	0.98	1.00		Sakino <i>et al.</i> (2004)
CR8-C-4-1	4493	0.95	0.96	0.99		
CR8-C-4-2	4542	0.96	0.97	1.00		
CR8-C-8	5366	0.95	0.95	1.00	Mursi and Uy (2004)	
CR4-A-4-3	3183	1.16	1.11	1.21		
CR4-A-9	4773	1.02	0.96	1.08		
CR6-A-4-3	5898	1.10	1.12	1.16		

Table 7 Continued

Specimens	P_{exp} (kN)	$P_{exp}/P_{u.sqr}$	$P_{exp}/P_{u.AS5100.6}$	$P_{exp}/P_{u.EC4}$	Ref.
CR6-A-9	7008	0.95	0.97	1.04	Sakino <i>et al.</i> (2004)
CR6-C-4-3	4026	1.05	1.01	1.07	
CR6-C-9	5303	0.95	0.90	0.98	
CR8-C-4-3	5028	1.03	1.04	1.07	
CR8-C-9	5873	0.93	0.93	0.99	
SH-C160	2831	1.02	1.02	1.03	
A9-1	1739	1.08	1.08	1.16	Liu and Gho (2005)
A9-2	1718	1.07	1.07	1.14	
A12-1	1963	1.10	1.08	1.16	
A12-2	1988	1.12	1.09	1.17	
A1	1697	0.98	0.96	1.05	
A2	1919	0.96	0.94	1.04	
A3-1	3996	0.99	0.93	1.04	
A3-2	3862	0.96	0.90	1.00	
R1-1	1701	1.02	1.02	1.09	
R1-2	1657	0.99	0.99	1.06	
R4-1	2020	1.09	1.07	1.15	
R4-2	2018	1.09	1.07	1.15	
R7-1	1749	1.03	1.05	1.14	
R8-1	1752	1.03	1.06	1.14	
R10-1	2752	1.11	1.05	1.15	
R10-2	2828	1.14	1.08	1.18	
SA1-1	382	1.01	1.01	1.12	Han <i>et al.</i> (2005)
SA1-2	350	0.92	0.92	1.03	
SC1-1	422	0.96	0.96	1.05	
SC1-2	406	0.92	0.92	1.01	
4	1310	1.01	1.08	1.16	Zhang <i>et al.</i> (2005)
5	1340	1.01	1.07	1.15	
6	1370	1.05	1.12	1.20	
7	2160	1.01	1.02	1.11	
8	2250	1.05	1.07	1.16	
9	2280	1.08	1.09	1.19	
13	1500	1.01	1.09	1.17	
14	1330	0.92	0.99	1.07	
15	1440	0.99	1.07	1.15	
16	2520	1.05	1.07	1.17	
17	2610	1.09	1.10	1.21	Lam and Gardner (2008)
18	1700	0.74	0.75	0.82	
SHS150×150×6 -C80	3020	0.88	0.91	0.98	

Table 7 Continued

Specimens	P_{exp} (kN)	$P_{exp}/P_{u.sqr}$	$P_{exp}/P_{u.AS5100.6}$	$P_{exp}/P_{u.EC4}$	Ref.
NCFT160R	3449	0.98	1.00	1.04	Lee <i>et al.</i> (2009)
NCFT240R	6009	1.01	1.00	1.05	
L0	863	1.06	0.93	1.00	Chen <i>et al.</i> (2011)
H0	1354	0.97	1.07	1.18	
L0	1088	1.12	1.09	1.17	
H0	1469	1.06	1.11	1.21	
Pa-6-2	3010	1.07	1.07	1.11	Zhu <i>et al.</i> (2012)
CB20 - SH (A)	2524	1.07	1.22	1.27	Uy <i>et al.</i> (2013)
CB20 - SH (B)	2632	1.17	1.27	1.32	
CB 25 - SH (A)	3024	1.22	1.06	1.11	
CB 25 - SH (B)	2971	1.04	1.04	1.09	
CB 30 - SH (A)	4115	1.02	1.02	1.09	
CB 30 - SH (B)	3968	1.03	0.99	1.05	
CB 40 - SH (A)	5184	0.99	0.81	0.87	
CB40SH (B)	5604	0.88	0.87	0.94	
SC2B	1934	0.95	1.15	1.17	
SC3B	2348	1.14	1.09	1.12	
SC4B	2828	1.09	1.07	1.10	Aslani <i>et al.</i> (2015a)
HSSC1	2203	1.08	0.97	1.01	
HSSC2	2234	0.96	0.98	1.03	
HSSC3	2942	0.97	0.95	1.00	
HSSC4	2840	0.96	0.92	0.97	
HSSC5	3118	0.93	0.77	0.82	
HSSC6	3243	0.81	0.81	0.86	
HSSC7	3882	0.85	0.83	0.88	
HSSC8	3856	0.89	0.82	0.88	
Mean		1.00	1.01	1.07	
Standard Deviation (SD)		0.08	0.10	0.11	

8. Conclusions

The following conclusions can be made with the present scope of investigation:

- A reliable FEM model for the non-linear analysis of normal and high-strength short square and rectangular CFSTCs has been developed. The present model considers the effects of initial imperfections and residual stresses of steel tubes as well as the confinement effect of

Table 8 Comparison of results of AS5100.6 (2004), Eurocode 4 (2004), and proposed design model predicted ultimate axial strengths with test results for short square and rectangular CFSTCs

Ref.	S-NSS-TC-HSC		S-HSS-TC-NSC		S-HSS-TC-HSC	
	P_{exp}/P_{cal}		P_{exp}/P_{cal}		P_{exp}/P_{cal}	
	\bar{x}	$\bar{\sigma}$	\bar{x}	$\bar{\sigma}$	\bar{x}	$\bar{\sigma}$
AS5100.6 (2004)	1.01	0.09	0.97	0.10	1.01	0.10
Eurocode 4 (2004)	1.10	0.09	1.02	0.10	1.08	0.10
Proposed design model	\bar{x}	$\bar{\sigma}$	\bar{x}	$\bar{\sigma}$	\bar{x}	$\bar{\sigma}$
	1.00	0.07	0.99	0.08	1.01	0.07

Ref.	R-NSS-TC-HSC		R-HSS-TC-NSC		R-HSS-TC-HSC	
	P_{exp}/P_{cal}		P_{exp}/P_{cal}		P_{exp}/P_{cal}	
	\bar{x}	$\bar{\sigma}$	\bar{x}	$\bar{\sigma}$	\bar{x}	$\bar{\sigma}$
AS5100.6 (2004)	1.02	0.08	1.03	0.05	0.98	0.06
Eurocode 4 (2004)	1.11	0.07	1.09	0.05	1.05	0.6
Proposed design model	\bar{x}	$\bar{\sigma}$	\bar{x}	$\bar{\sigma}$	\bar{x}	$\bar{\sigma}$
	1.00	0.05	1.01	0.04	1.00	0.04

Table 9 Comparison of ultimate axial strengths of rectangular CFSTCs determined by experiment, design codes and proposed design model

Specimens	P_{exp} (kN)	$P_{exp}/P_{u.rec}$	$P_{exp}/P_{u.AS5100.6}$	$P_{exp}/P_{u.EC4}$	Ref.	
rc5-1	554	1.00	1.20	1.31	Han (2002)	
rc5-2	576	1.04	1.24	1.36		
rc6-1	640	1.01	1.19	1.31		
rc6-2	672	1.06	1.25	1.37		
rc7-1	800	0.97	1.09	1.21		
rc7-2	760	0.92	1.04	1.15		
rc11-1	760	0.91	1.01	1.12		
rc11-2	820	0.98	1.10	1.21		
rc12-1	880	1.05	1.16	1.28		
rc12-2	740	0.88	0.97	1.07		
C5-1	1450	0.97	1.00	1.06		Liu <i>et al.</i> (2003)
C5-2	1425	0.95	0.98	1.04		
C6-1	1560	0.98	1.01	1.08		
C6-2	1700	1.06	1.10	1.17		
C7-1	2530	0.98	0.93	1.01		
C8-1	2970	1.08	1.02	1.11		
C8-2	2590	0.94	0.89	0.96		
C9-1	1710	0.92	0.92	0.98		
C9-2	1820	0.99	0.98	1.05		
C10-1	1880	0.96	0.95	1.02		

Table 9 Continued

Specimens	P_{exp} (kN)	$P_{exp}/P_{u.rec}$	$P_{exp}/P_{u.AS5100.6}$	$P_{exp}/P_{u.EC4}$	Ref.	
C10-2	2100	1.07	1.07	1.15	Liu <i>et al.</i> (2003)	
C11-1	2350	0.96	0.90	0.97		
C11-2	2380	0.98	0.93	1.00		
C12-1	2900	1.10	1.03	1.12		
C12-2	2800	1.07	1.01	1.10		
A10-1	1815	1.08	1.08	1.16	Liu and Gho (2005)	
A10-2	1763	1.05	1.05	1.12		
A11-1	1725	0.98	0.95	1.02		
A11-2	1742	0.99	0.96	1.03		
A13-1	1947	1.05	1.03	1.10		
A13-2	1912	1.03	1.01	1.08		
A14-1	2035	1.05	1.00	1.07		
A14-2	2138	1.10	1.05	1.13		
A4-1	1601	0.98	0.98	1.07		
A4-2	1566	0.96	0.96	1.05		
A5-1	1854	0.99	0.99	1.09		
A5-2	1779	0.95	0.95	1.04		
A6-1	3684	0.94	0.91	1.01		
A6-2	3717	0.95	0.92	1.02		
A7-1	2059	0.96	0.95	1.04		
A7-2	2019	0.94	0.93	1.02		
A8-1	2287	0.92	0.91	1.01		
A8-2	2291	0.92	0.91	1.01		
R2-1	1735	1.00	1.00	1.07		Liu (2005)
R2-2	1778	1.02	1.02	1.09		
R3-1	1773	0.97	0.94	1.01		
R3-2	1795	0.98	0.95	1.02		
Specimens	P_{exp} (kN)	$P_{exp}/P_{u.rec}$	$P_{exp}/P_{u.AS5100.6}$	$P_{exp}/P_{u.EC4}$	Ref.	
R5-1	1982	1.03	1.01	1.08	Liu (2005)	
R5-2	1923	1.00	0.98	1.05		
R6-1	2049	1.02	0.97	1.04		
R6-2	2124	1.05	1.00	1.08		
R7-2	1824	1.02	1.05	1.14		
R8-2	1806	0.95	0.95	1.03		
R9-1	1878	1.05	1.09	1.18		
R9-2	1858	0.98	0.98	1.06		
R11-1	2580	1.01	0.96	1.06		
R11-2	2674	1.04	1.00	1.09		

Table 9 Continued

Specimens	P_{exp} (kN)	$P_{exp}/P_{u.rec}$	$P_{exp}/P_{u.AS5100.6}$	$P_{exp}/P_{u.EC4}$	Ref.
25	1875	1.03	1.06	1.15	
26	1915	1.07	1.11	1.20	
27	1820	0.99	1.02	1.11	
28	1580	0.99	1.06	1.14	
29	1600	0.98	1.05	1.14	
30	1640	1.01	1.08	1.16	
31	2510	1.05	1.07	1.17	
32	2470	1.03	1.05	1.14	Zhang <i>et al.</i> (2005)
33	2260	0.98	0.97	1.06	
34	2510	1.09	1.08	1.18	
41	1840	1.04	1.13	1.23	
42	1820	1.02	1.10	1.19	
43	1725	0.96	1.03	1.12	
44	2090	1.05	1.09	1.19	
45	2320	1.10	1.13	1.24	
46	2060	1.03	1.06	1.16	
47	2600	0.97	0.99	1.08	Lam and Gardner (2008)
48	2700	1.01	1.02	1.13	
49	2700	1.05	1.02	1.12	
50	2680	1.04	1.03	1.13	
RHS 200 × 110 × 4 – C80	2180	1.06	0.82	0.90	
RHS 140 × 80 × 3 – C80	1259	1.06	0.87	0.95	
RAC-36-30	4017	0.89	1.12	1.15	Hong <i>et al.</i> (2013)
Mean	1.00	1.02	1.10		
Standard deviation (SD)	0.05	0.08	0.09		

the concrete infill. Meanwhile, a new confined concrete equivalent stress-strain relationship was developed to be used in modelling of CFSTCs.

- The FEM verification studies show that the proposed relationship can accurately predict the ultimate axial strength and behaviour of high-strength steel box composite columns.
- Simplified maximum compressive strengths of confined concrete models are proposed that can predict the confining pressure for the normal and high-strength short square and rectangular CFSTCs with B/t ratios, f_c and f_y in the range of 15–52, 20–110 N/mm², and 220–850 N/mm², respectively.
- A convenient design model for predicting the ultimate axial strengths was proposed for short square and rectangular CFSTCs. Proposed design models yield accurate predictions for the ultimate axial strengths of axially loaded composite sections.

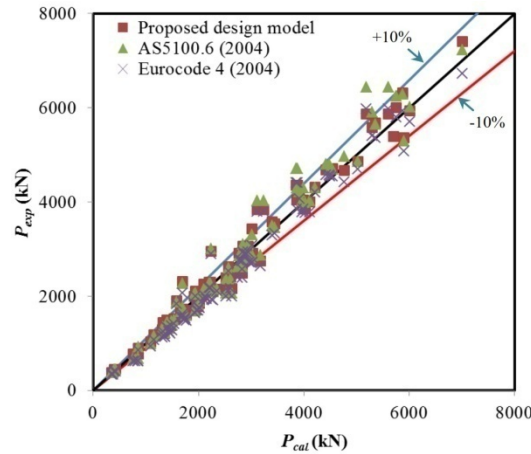


Fig. 14 Comparison between proposed design model, AS5100.6 (2004), and Eurocode 4 (2004) predictions and experimental ultimate strengths for short square CFSTCs

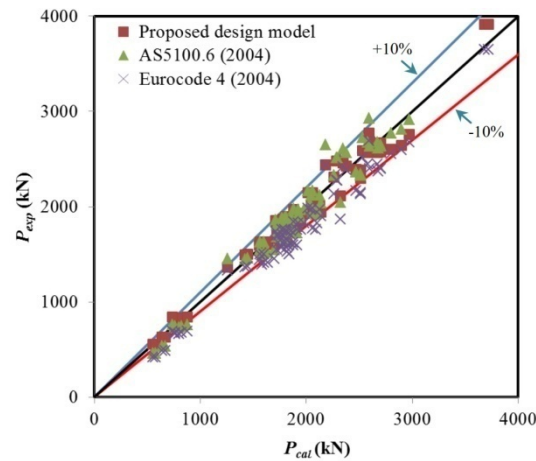


Fig. 15 Comparison between proposed design model, AS5100.6 (2004), and Eurocode 4 (2004) predictions and experimental ultimate strengths for short rectangular CFSTCs

- Test strengths for short box composite sections were compared with AS5100.6 and Eurocode 4. These were shown to be conservative for most of the high-strength box composite columns. Thus, they are considered suitable for design.
- Further research is needed to extend the generic confinement model for the concrete core in triangular, fan-shaped, D-shaped, quadri-circular, and semi-circular concrete-filled steel tubular short columns.

References

ABAQUS (2013), ABAQUS Standard User’s Manual, Version 6.13, Dassault Systèmes Corp., Providence, RI, USA.

- American Concrete Institute (ACI) (2010), Building code requirements for structural concrete and commentary; ACI 318-10. Farmington Hills, MI, USA.
- AS 5100.6 (2004), Bridge design Part 6: Steel and composite construction, Standards Australia, Sydney, New South Wales, Australia.
- Aslani, F. (2013), "Effects of specimen size and shape on compressive and tensile strengths of self-compacting concrete with or without fibers", *Magaz. Concrete Res.*, **65**(15), 914-929.
- Aslani, F., Uy, B., Tao, Z. and Mashiri, F. (2015a), "Behaviour and design of composite columns incorporating compact high-strength steel plates", *J. Construct. Steel Res.*, **107**, 94-110.
- Aslani, F., Uy, B., Tao, Z. and Mashiri, F. (2015b), "Predicting the axial load capacity of high-strength concrete filled steel tubular columns", *Steel Compos. Struct., Int. J.*, **19**(4), 967-993.
- Aslani, F., Lloyd, R., Uy, B., Kang, W.H. and Hicks, S. (2016), "Statistical calibration of safety factors for flexural stiffness of composite columns", *Steel Compos. Struct., Int. J.*, **20**(1), 127-145.
- Aslani, F., Uy, B., Hur, J. and Carino, P. (2017), "Behaviour and design of hollow and concrete-filled spiral welded steel tube columns subjected to axial compression", *J. Constr. Steel Res.*, **128**, 261-288.
- Bazant, Z.P. and Becq-Giraudon, E. (2002), "Statistical prediction of fracture parameters of concrete and implications for choice of testing standard", *Cem. Concr. Res.*, **32**(4), 529-556.
- Chen, Z.Y. and Shen, Z.Y. (2010), "Behavior of L-shaped concrete-filled steel stub columns under axial loading: experiment", *Adv. Steel Constr.*, **6**(2), 688-697.
- Chen, B., Liu, X. and Li, S. (2011), "Performance investigation of square concrete-filled steel tube columns", *J. Wuhan Univ. Tech.*, **24**(4), 730-736.
- Chen, C.C., Ko, J.W., Huang, G.L. and Chang, Y.M. (2012), "Local buckling and concrete confinement of concrete-filled box columns under axial load", *J. Constr. Steel Res.*, **78**, 8-21.
- Eurocode 4 (2004), Design of composite steel and concrete structures; Part 1.1, General rules and rules for Building, BS EN 1994-1-1: British Standards Institution, London, UK.
- FIP (2010), CEB-FIP Model Code 2010, Thomas Telford Ltd., London, UK.
- Fujimoto, T., Nishiyama, I., Mukai, A. and Baba, T. (1995), "Test results of eccentrically loaded short columns—square CFT columns", *Proceedings of the Second Joint Technical Coordinating Committee Meeting on Composite and Hybrid Structures*, Hawaii, USA.
- Guo, L., Zhang, S., Kim, W.J. and Ranzi, G. (2007), "Behavior of square hollow steel tubes and steel tubes filled with concrete", *Thin-Wall. Struct.*, **45**(12), 961-973.
- Han, L.H. (2002), "Tests on stub columns of concrete-filled RHS sections", *J. Constr. Steel Res.*, **58**(3), 353-372.
- Han, L.H., Yao, G.H. and Zhao, X.L. (2005), "Tests and calculations for hollow structural steel (HSS) stub columns filled with self-consolidating concrete (SCC)", *J. Constr. Steel Res.*, **61**(9), 1241-1269.
- Hernández-Figueirido, D., Romero, M.L., Bonet, J.L. and Montalvá, J.M. (2012), "Ultimate capacity of rectangular concrete-filled steel tubular columns under unequal load eccentricities", *J. Constr. Steel Res.*, **68**(1), 107-117.
- Hong, G., Kim, W., Choi, I. and Chung, K. (2013), "Structural performance of high strength concrete filled steel tube with the width-to-thickness ratio", *Appl. Mech. Mater.*, **284-287**, 1390-1395.
- Johansson, M. and Gylltoft, K. (2001), "Structural behavior of slender circular steel-concrete composite columns under various means of load application", *Steel Compos. Struct., Int. J.*, **1**(4), 393-410.
- Kilpatrick, A.E. and Rangan, B.V. (1999a), "Tests on high-strength concrete-filled steel tubular columns", *ACI Struct. J.*, **96**(2), 268-274.
- Kilpatrick, A.E. and Rangan, B.V. (1999b), "Influence of interfacial shear transfer on behavior of concrete-filled steel tubular columns", *ACI Struct. J.*, **96**(4), 642-648.
- Lam, D. and Gardner, L. (2008), "Structural design of stainless steel concrete filled columns", *J. Constr. Steel Res.*, **64**(11), 1275-1282.
- Lee, M.J., Oh, Y.S. and Lee, E.T. (2009), "Examination of yield stress limitation for concrete filled steel tube (CFT) column using SM570TMC steel", *Tubular Structures XII*, 93-102.
- Liu, D.L. (2004), "Behaviour of high strength rectangular concrete-filled steel hollow section columns under eccentric loading", *Thin-Wall. Struct.*, **42**(12), 1631-1644.

- Liu, D.L. (2005), "Tests on high-strength rectangular concrete-filled steel hollow section stub columns", *J. Constr. Steel Res.*, **61**(7), 902-911.
- Liu, D.L. (2006), "Behaviour of eccentrically loaded high-strength rectangular concrete-filled steel tubular columns", *J. Constr. Steel Res.*, **62**(8), 839-846.
- Liu, D. and Gho, W.M. (2005), "Axial load behaviour of high-strength rectangular concrete-filled steel tubular stub columns", *Thin-Wall. Struct.*, **43**(8), 1131-1142.
- Liu, D., Gho, W.M. and Yuan, J. (2003), "Ultimate capacity of high-strength rectangular concrete-filled steel hollow section stub columns", *J. Constr. Steel Res.*, **59**(12), 1499-1515.
- Melcher, J.J. and Karmazinova, M. (2004), "The analysis of composite steel-and concrete compression members with high-strength concrete", *Proceedings of SSRC annual technical session*, 223-237.
- Mursi, M. and Uy, B. (2004), "Strength of slender concrete filled high strength steel box columns", *J. Constr. Steel Res.*, **60**(12), 1825-1848.
- Mursi, M. and Uy, B. (2006a), "Behaviour and design of fabricated high strength steel columns subjected to biaxial bending, Part 1: Experiments", *Int. J. Adv. Steel Constr.*, **2**(4), 286-315.
- Mursi, M. and Uy, B. (2006b), "Behaviour and design of fabricated high-strength steel columns subjected to biaxial bending, Part 2: Analysis and design codes", *Int. J. Adv. Steel Constr.*, **2**(4), 316-354.
- Packer, J.A. and Henderson, J.E. (2003), "Hollow structural section connections and trusses—A design guide", Canadian Institute of Steel Construction (CISC), Toronto, Canada.
- Portolés, J.M., Romero, M.L., Filippou, F.C. and Bonet, J.L. (2011), "Simulation and design recommendations of eccentrically loaded slender concrete-filled tubular columns", *Eng. Struct.*, **33**(5), 1576-1593.
- Rangan, B.V. and Joyce, M. (1992), "Strength of eccentrically loaded slender steel tubular columns filled with high-strength concrete", *ACI Struct. J.*, **89**(6), 676-681.
- Ren, Q.X., Han, L.H., Lam, D. and Hou, C. (2014), "Experiments on special-shaped CFST stub columns under axial compression", *J. Constr. Steel Res.*, **98**, 123-133.
- Sakino, K., Nakahara, H., Morino, S. and Nishiyama, I. (2004), "Behavior of centrally loaded concrete-filled steel-tube short columns", *J. Struct. Eng.-ASCE*, **130**(2), 180-188.
- Susantha, K.A.S., Ge, H. and Usami, T. (2001), "Uniaxial stress-strain relationship of concrete confined by various shaped steel tubes", *Eng. Struct.*, **23**(10), 1331-1347.
- Uy, B. (1998), "Local and post-local buckling of concrete filled steel welded box columns", *J. Constr. Steel Res.*, **47**(1-2), 47-72.
- Uy, B. (1999), "Axial compressive strength of steel and composite columns fabricated with high-strength steel plate", *Proceedings of the Second International Conference on Advances in Steel Structures*, Hong Kong, pp. 421-428.
- Uy, B. (2001a), "Strength of short concrete filled high strength steel box columns", *J. Constr. Steel Res.*, **57**(2), 113-134.
- Uy, B. (2001b), "Axial compressive strength of short steel and composite columns fabricated with high strength steel plate", *Steel Compos. Struct., Int. J.*, **1**(2), 171-185.
- Uy, B., Mursi, M. and Tan, A. (2002), "Strength of slender composite columns fabricated with high-strength structural steel", *Proceedings of the 3rd International Conference on Advances in Steel Structures ICASS'02*, Hong Kong, December, pp. 575-582.
- Uy, B., Khan, M., Tao, Z. and Mashiri, F. (2013), "Behaviour and design of high-strength steel concrete filled columns", *Proceedings of the 2013 World Congress on Advances in Structural Engineering and Mechanics (ASEM13)*, Jeju, Korea, pp. 150-167.
- Yang, H., Lam, D. and Gardner, L. (2008), "Testing and analysis of concrete-filled elliptical hollow sections", *Eng. Struct.*, **30**(12), 3771-3781.
- Yang, Y.L., Yang, H. and Zhang, S.M. (2010), "Compressive behavior of T-shaped concrete filled steel tubular columns", *Int. J. Steel Struct.*, **10**(4), 419-430.
- Yi, S.T., Yang, E.I. and Choi, J.C. (2006), "Effect of specimen sizes, specimen shapes, and placement directions on compressive strength of concrete", *Nucl. Eng. Des.*, **232**(2), 115-127.
- Yu, Q., Tao, Z. and Wu, Y.X. (2008), "Experimental behaviour of high performance concrete-filled steel

- tubular columns”, *Thin-Wall. Struct.*, **46**(4), 362-370.
- Zhang, S., Guo, L., Ye, Z. and Wang, Y. (2005), “Behavior of steel tube and confined high strength concrete for concrete-filled RHS tubes”, *Adv. Struct. Eng.*, **8**(2), 101-116.
- Zhu, A.Z., Luo, L.L. and Zhu, H.P. (2012), “Experimental study on concrete-filled cold-formed steel tubular stub columns”, *Tubular Structures XIV*, 73-80.

DL